

AN AUTOMATIC ANTISKID BRAKING CONTROL SYSTEM
FOR THE SPACE SHUTTLE VEHICLE

A Thesis Presented to
The Department of Electrical Engineering
University of Houston

In Partial Fulfillment
of the Requirements for the
Master of Science Degree

by
Guy S. Pennington, Jr.

May, 1974

ACKNOWLEDGEMENTS

I take this opportunity to acknowledge the guidance and support received from Dr. Eugene Denman, Professor of Electrical Engineering and Chairman of the Thesis Committee.

Also, a special note of appreciation to my wife Barbara who typed this manuscript, to my son Michael who helped plot data, and to my son John who helped in his own special way.

To my wife Barbara, and my sons
Michael and John. Without their
support and understanding this task
could not have been completed. This
was truly a family affair.

AN AUTOMATIC ANTISKID BRAKING CONTROL SYSTEM
FOR THE SPACE SHUTTLE VEHICLE

An Abstract of a Thesis
Presented to
The Department of Electrical Engineering
University of Houston

In Partial Fulfillment
of the Requirements for the
Master of Science Degree

by
Guy S. Pennington, Jr.
May, 1974

ABSTRACT

Large high-speed aircraft such as the Space Shuttle Vehicle require automatic antiskid braking control to prevent excessive tire wear and/or catastrophic failure during landing rollout. This thesis investigates the basic multiwheel braking problem, and presents an essentially all digital controller. The control system will accomplish totally automatic rollout braking control, or can be used simply for antiskid protection during pilots manual braking. Wheel speed and measured braking reaction torque are the feedback signals used for skid detection and prevention. Wheel slip is the basic control command variable. Simplified math models for vehicle dynamics, wheel/runway interface, and braking control system components were developed to test the control system design. These models were programmed in an all digital simulation, and typical test results are presented.

TABLE OF CONTENTS

CHAPTER	PAGE
1. INTRODUCTION	1
1.1 Antiskid Braking for the Space Shuttle Vehicle	1
1.2 A Brief History of Aircraft Skid Control Systems.....	3
2. PERFORMANCE REQUIREMENTS AND VEHICLE MATH MODEL.....	4
2.1 Performance Requirements (Design Considerations).....	4
2.2 Mathematical Models and Digital Computer Simulation -	5
General.....	5
2.3 Model for Wheel Dynamics and Tire/Runway Interface....	5
2.4 Vehicle Dynamics Math Model.....	14
2.5 Vehicle Translational Equations of Motion.....	16
2.6 Vehicle Rotational Equations of Motion.....	20
2.7 Digital Computer Simulation and CSMP.....	24
3. DESIGN OF AN AUTOMATIC ANTISKID BRAKING CONTROL SYSTEM.....	29
3.1 Design Approaches and the Friction Slip Curve.....	29
3.2 An Automatic Antiskid Braking Control System:	31
Functional Description.....	31
3.3 Slip Command Controller with Rollout Estimator.....	32
3.4 Brake Pressure UP/DOWN Counter and Counter Control	35
Logic.....	35
3.5 Digital Filter.....	41
3.6 D/A Converter.....	45
3.7 Brake Pressure Control Valve.....	48

CHAPTER	PAGE
3.8 Disc Brake System.....	48
3.9 Wheel Speed Transducers and Torque Transducers.....	49
3.10 Mu-Slip Peak Detector and Maximum Slip Limiter.....	49
3.11 Steering Control Law.....	56
3.12 Cockpit Controls and Displays.....	58
4. TESTING, RESULTS, AND CONCLUSIONS.....	60
4.1 System Testing.....	60
4.2 Results.....	62
4.3 Conclusions.....	68

LIST OF TABLES

TABLE	PAGE
1. PARTIAL LISTING OF SPECIAL CSMP FUNCTIONS	25
2. COEFFICIENT DATA FOR A FIRST ORDER DIGITAL FILTER	45

LIST OF FIGURES

FIGURE	PAGE
1. TYPICAL FRICTION-SLIP CHARACTERISTIC OF AN AIRCRAFT TIRE AT ROLLOUT VELOCITY.....	2
2. SPACE SHUTTLE VEHICLE OUTLINE AND DIMENSIONAL DATA.....	6
3. MAIN LANDING GEAR STRUT CONFIGURATION.....	7
4. MATHEMATICAL MODEL FOR WHEEL AND TIRE/RUNWAY INTERFACE....	8
5. TYPICAL PRESSURE SERVOVALVE STEP RESPONSE CHARACTERISTIC FOR 100% COMMAND.....	9
6. BRAKE TORQUE VS BRAKE PRESSURE CURVE.....	10
7. A FAMILY OF MU-SLIP CURVES.....	13
8. RELATIVE ORIENTATION OF LANDING SYSTEM AND BODY AXIS COORDINATE SYSTEMS.....	15
9. RESOLUTION OF BODY FORCES INTO LANDING SYSTEM COORDINATES.	16
10. AERODYNAMIC DRAG FORCE (F_D) AS A FUNCTION OF TOTAL VELOCITY (V_T).....	18
11. DRAG CHUTE EFFECTIVENESS DATA.....	19
12. ^a RUDDER TORQUE EFFECTIVENESS AS A FUNCTION OF VELOCITY.....	22
12. ^b RUDDER TORQUE EFFECTIVENESS AS A FUNCTION OF RUDDER POSITION.....	22
13. NOSEWHEEL COEFFICIENT OF FRICTION AS A FUNCTION OF STEERING ANGLE.....	23
14. SIMPLIFIED SOFTWARE FLOW DIAGRAM FOR TIRE/RUNWAY INTER- FACE MODEL.....	26

FIGURE	PAGE
15. SIMPLIFIED SOFTWARE FLOW DIAGRAM FOR THE VEHICLE DYNAMICS MATH MODEL.....	27
16. AREAS OF CONTROL FOR VARIOUS CONTROL SCHEMES.....	29
17. FUNCTIONAL BLOCK DIAGRAM OF AUTOMATIC ANTISKID BRAKING CONTROL SYSTEM.....	33
18. ROLLOUT ESTIMATOR PARAMETERS.....	34
19. FLOW DIAGRAM FOR ROLLOUT ESTIMATOR AND SLIP COMMAND CONTROLLER.....	36
20. MASTER UP/DOWN COUNTER SOFTWARE FLOW DIAGRAM.....	37
21. BRAKE PRESSURE UP/DOWN COUNTER AND CONTROL LOGIC.....	39
22. GAIN-VS-FREQUENCY CURVE FOR $A/(S+A)$ TRANSFER FUNCTION.....	42
23. S DOMAIN REPRESENTATION OF DIGITAL FILTER.....	42
24. BLOCK DIAGRAM FOR FIRST ORDER LAG DIGITAL FILTER.....	44
25. RESPONSE OF DIGITAL FILTER TO EXPONENTIAL + 5 HZ SINUSOID.	46
26. TYPICAL RESPONSE OF A FIRST ORDER DIGITAL FILTER TO A STEP INPUT.....	47
27. BRAKE PRESSURE CONTROL VALVE BLOCK DIAGRAM.....	48
28. A FAMILY OF MU-SLIP CURVES.....	49
29. TYPICAL μ AND $d\mu/d\sigma$	52
30. SYSTEM PERFORMANCE IN AUTOMATIC MODE.....	63
31. MU AND SLIP DATA FOR PEAK RIDING PERFORMANCE ON WET RUNWAY.....	64
32. MU AND SLIP RESPONSE DATA FOR FIXED SLIP COMMAND OPERATION (SLIP COMMAND = .25).....	65

FIGURE	PAGE
33. MU AND SLIP RESPONSE FOR SYSTEM OPERATION WITH COMPUTED CANCELLATION OF $J \dot{\omega}$ TERM (10000/SEC PEAK CHECK).....	67
34. MU AND SLIP RESPONSE FOR SYSTEM OPERATION (100/SEC PEAK CHECK).....	67
35. TYPICAL WHEEL LOCKUP CHARACTERISTIC WITH EXCESSIVE BRAKING PRESSURE APPLIED.....	69
36. STEERING CONTROL EFFECTIVENESS DATA.....	70
37. STEERING VIA MAIN GEAR BRAKING.....	71

CHAPTER 1

INTRODUCTION

1.1 Antiskid Braking for the Space Shuttle Vehicle

The subject of this thesis is the design and evaluation of an automatic antiskid braking control system for the Space Shuttle Vehicle. This vehicle is currently under development by the National Aeronautics and Space Administration (NASA), and is approximately equal in size to present day large jet transport aircraft. Focus of the thesis is on the basic braking control system problem: other topics such as cost, reliability, redundancy management, materials, and structures are omitted, although they are certainly part of the total design problem.

Automatic antiskid braking is required on most large aircraft for the simple reason that the pilot, when depressing the braking control footpedal, has very little physical indication of actual wheel behavior. Thus, a wheel may "lock up" during braking, and skid several hundred feet down the runway before the pilot is aware of it and releases pressure. The result is excessive tire wear or blowout. The problem is particularly acute on very large aircraft such as the Lockheed C-5A or the Boeing 747, which can have as many as sixteen braked wheels. The automatic antiskid system philosophy developed in this thesis could be applied to such aircraft, in addition to the Space Shuttle.

The design basis for an automatic antiskid braking control system is the tire/runway interface characteristic. This interface is the

point at which braking forces are realized, and at which two fundamental control variables are active: friction and wheel slip. Effective friction and wheel slip are related to each other by a function which typically can be characterized by a curve of the following form: ^(1,2,3)

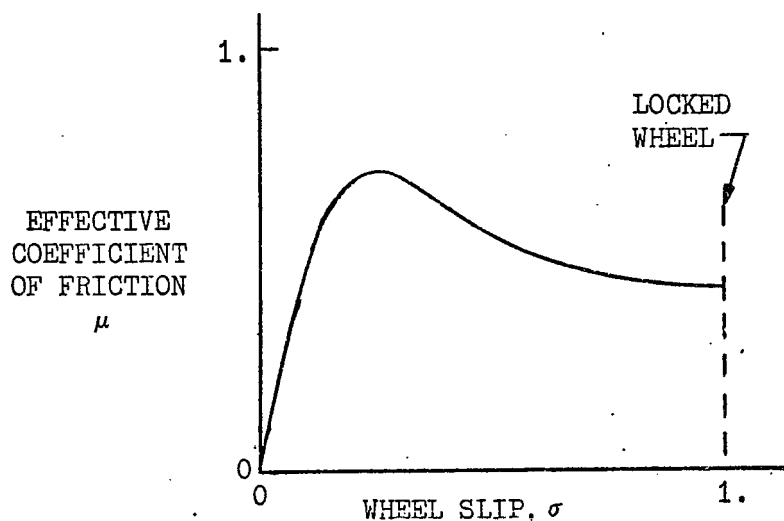


FIGURE 1.. TYPICAL FRICTION-SLIP CHARACTERISTIC OF AN AIRCRAFT TIRE AT ROLL-OUT VELOCITY.

The shape of this curve is influenced by many factors, including runway surface (concrete, asphalt), condition of surface (wet, dry, ice, sandy, etc.), tire condition (new, worn, tread pattern), aircraft velocity down runway, and temperature. A detailed discussion of the curve, the μ and slip variables, and design approaches based upon the general shape of the curve is presented in Chapters 2 and 3.

The control system developed in this thesis is essentially all digital. Thus it can be readily implemented on the Space Shuttle Vehicle since there is extensive digital computer capability on board.

These computers perform autopilot, guidance, navigation, and monitoring functions during orbital and aerodynamic flight.

Mathematical models for vehicle and wheel dynamics, and for braking control system components, were developed and programmed in an all digital simulation. An IBM 360/44 digital computer in the Engineering Systems Simulation Laboratory at the University of Houston was used for all program runs.

1.2 A Brief History of Aircraft Skid Control Systems (2)

In the early 1950's, antiskid systems were basically on-off (bang-bang) controllers. Wheel deceleration was the sensed control variable, with full hydraulic braking pressure applied until a deceleration threshold was exceeded, then dumped to near zero (return line pressure) until deceleration dropped below the threshold. Methods of detecting wheel deceleration included flywheel inertial acceleration sensors and differentiated outputs of electrical wheel speed sensors.

In the late 1950's and early 1960's systems were developed which modulated brake pressure within some operating range. Electrical wheel speed sensors were used, with output differentiated to provide a wheel deceleration signal. Closed loop brake pressure control was mechanized.

From the late 1960's to the present, several schemes have been developed which control wheel slip and wheel speed via closed loop control of brake pressure.

CHAPTER 2 :

PERFORMANCE REQUIREMENTS AND VEHICLE MATH MODEL

2.1 Performance Requirements (Design Considerations)⁽⁵⁾

The Shuttle braking system is required to stop the vehicle within a rollout distance of 6000 feet while preventing excessive tire wear (or failure), and without causing loss of directional stability. This must be accomplished either with or without benefit of a drag chute. Velocity at touchdown will be approximately 300 feet per second, and brakes can be applied as soon as all wheels are on the runway. The vehicle has two main landing gear struts, each with two wheels, and a nose gear. Only the four main landing gear wheels have brakes; the nose gear is used for steering.

On board avionics gear which can be used to provide data for braking and rollout control include:

- Inertial Measurement Unit (IMU). Provides vehicle attitude (pitch, roll, yaw) information with respect to runway coordinate system.
- Accelerometers, mounted in the IMU. These signals are numerically integrated in the guidance and control computers to obtain vehicle velocity and position information.
- Body mounted rate gyroscopes. Provides measurement of pitch, roll, and yaw body rates.
- Wheel speed sensors.
- Digital computers. Available for execution of control routines.

- Ground speed and distance measuring equipment.

Figure 2 depicts the basic Shuttle vehicle outline, and some dimensions of interest. Mass of the vehicle at touchdown will be 155,000 to 187,000 pounds. Approximate moment of inertia are:

$$I_{xx} = 7.5 \times 10^6 \text{ slug-ft}^2$$

$$I_{yy} = 5.3 \times 10^6 \text{ slug-ft}^2$$

$$I_{zz} = 5.5 \times 10^6 \text{ slug-ft}^2$$

2.2 Mathematical Models and Digital Computer Simulation - General.

Mathematical models of the Shuttle vehicle and the tire/runway interface were developed in order to evaluate performance of the automatic antiskid braking system. The models were programmed in an all digital simulation using a combination of FORTRAN and IBM's Continuous System Modeling Program (CSMP).⁽⁶⁾ All simulation runs were made at the University of Houston's Engineering Systems Simulation Laboratory on an IBM 360/44 machine. Some features of the CSMP language are discussed later in this Chapter. FORTRAN is a widely known program language and is not reviewed.

2.3 Model for Wheel Dynamics and Tire/Runway Interface.

Figure 3 shows the basic main landing gear strut configuration. The corresponding mathematical model, including the tire/runway interface, is shown in Figure 4. Individual elements (blocks) of the diagram in Figure 4 are discussed next.

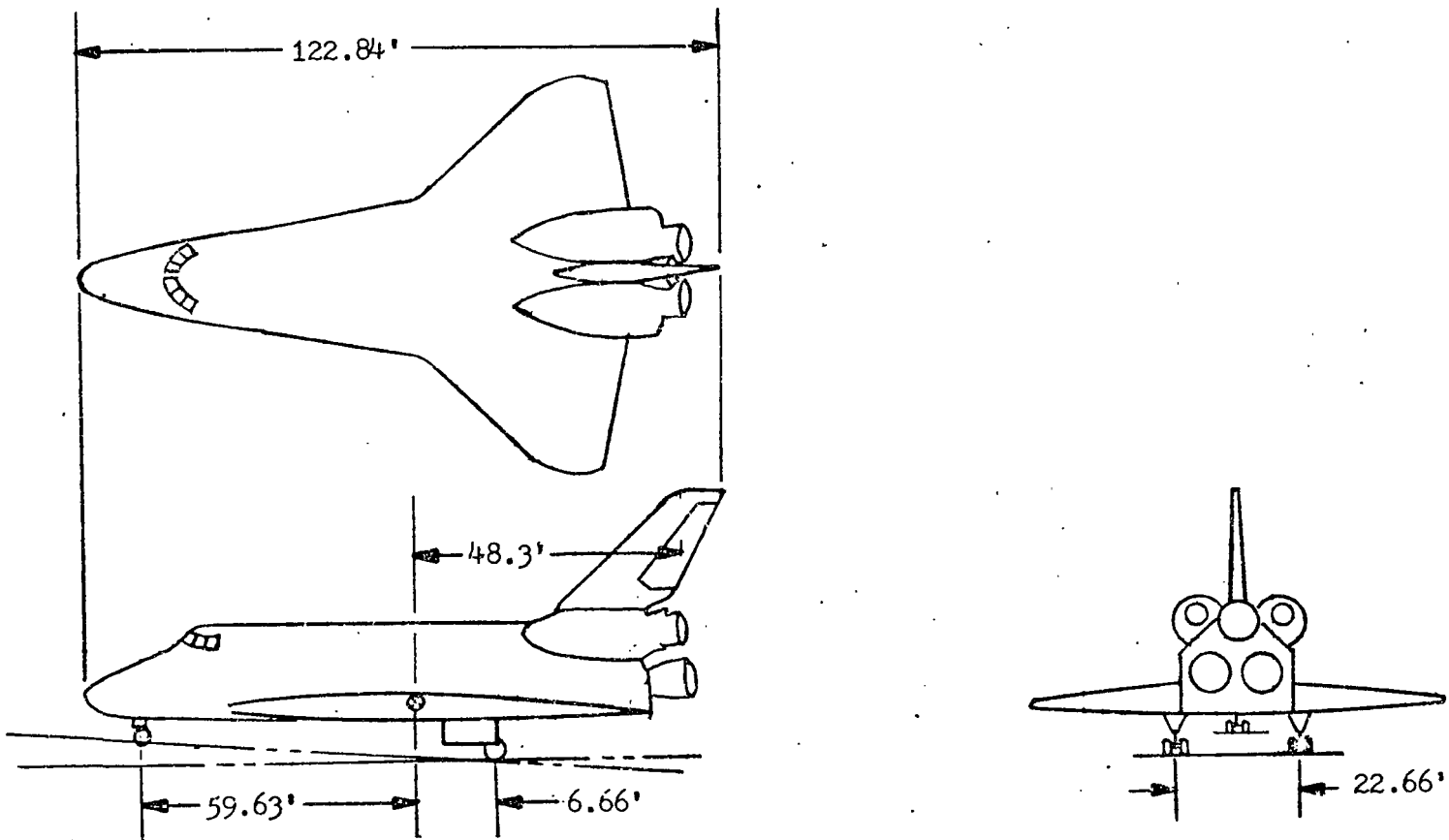


FIGURE 2. SPACE SHUTTLE VEHICLE OUTLINE AND DIMENSIONAL DATA.

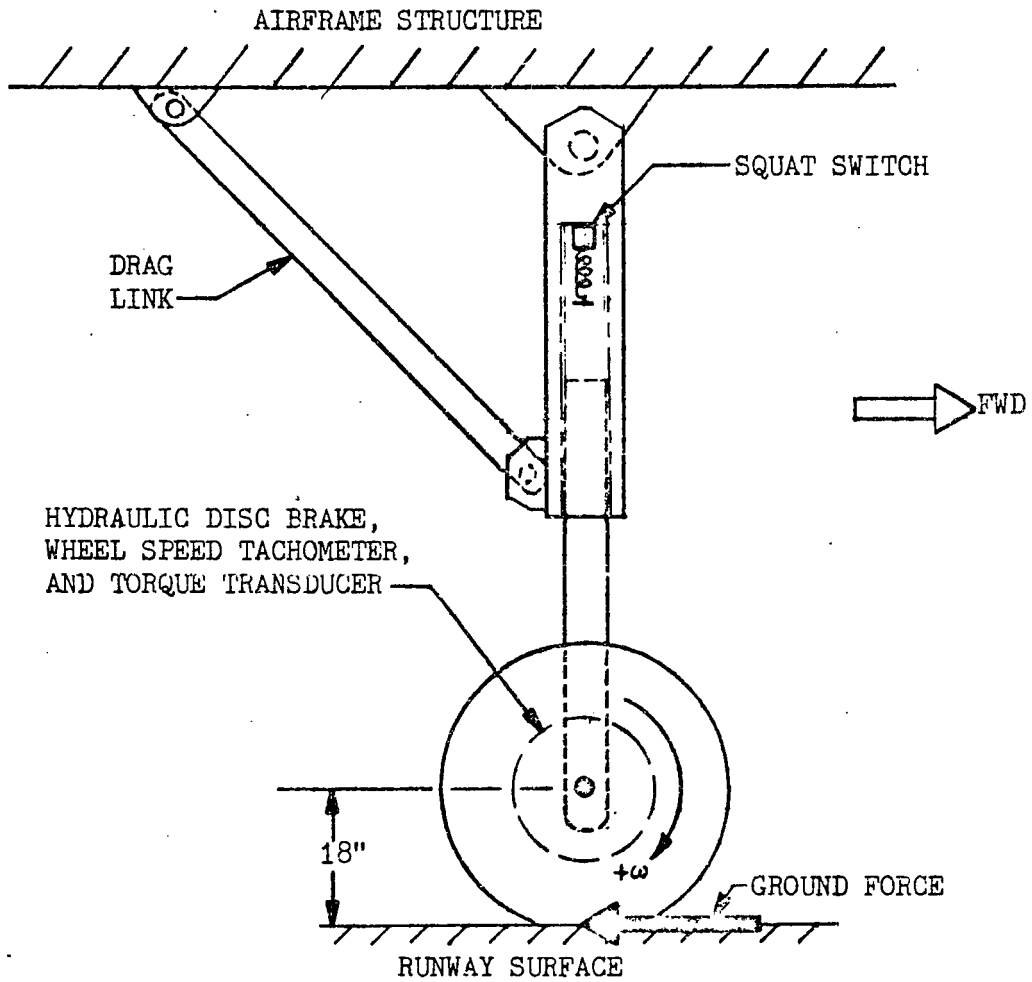
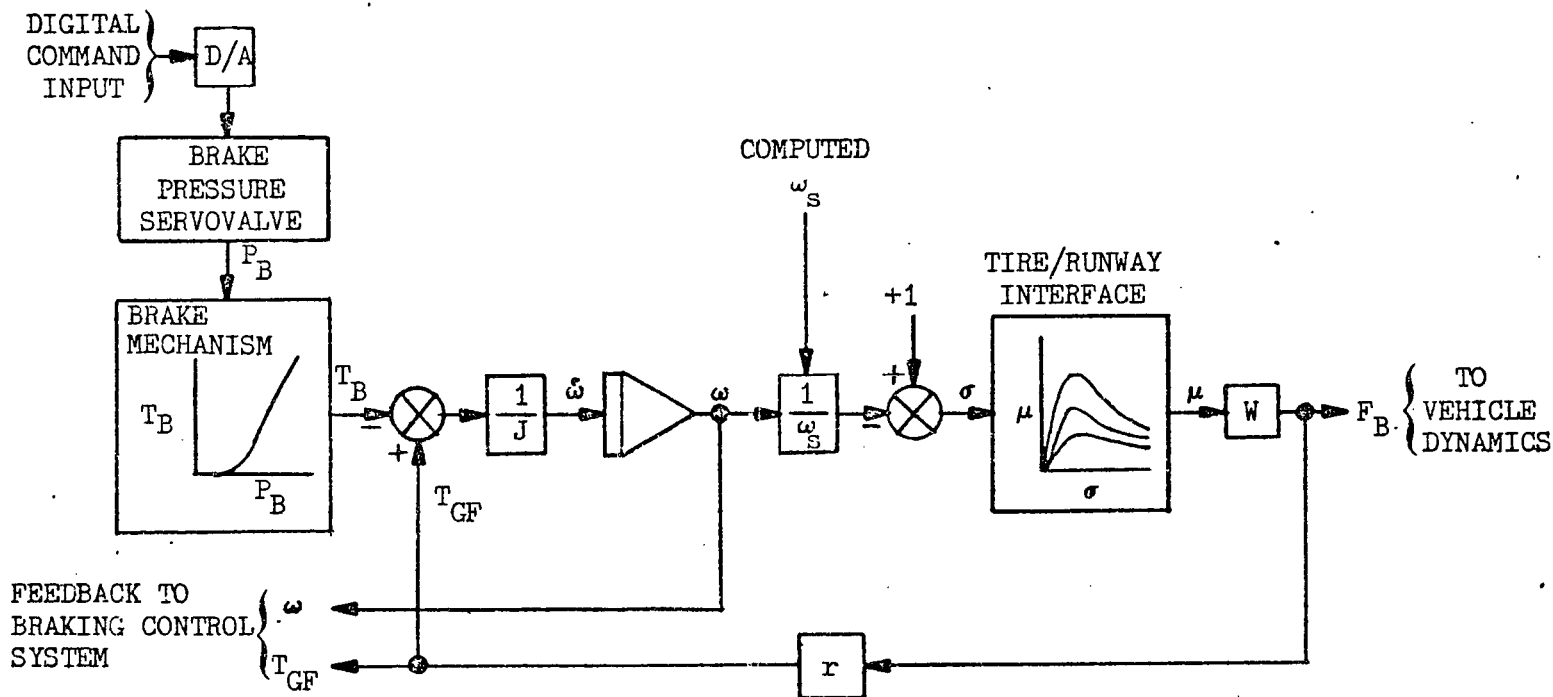


FIGURE 3. MAIN LANDING GEAR STRUT CONFIGURATION.



- | | |
|--|---------------------------------|
| T_B = BRAKING TORQUE | W = WEIGHT SUPPORTED BY WHEEL |
| P_B = HYDRAULIC BRAKE PRESSURE | F_B = NET BRAKING FORCE |
| J = MOMENT OF INERTIA OF WHEEL | r = ROLLING RADIUS OF WHEEL |
| $\dot{\omega}, \omega$ = WHEEL ROTATIONAL ACCELERATION, VELOCITY | T_{GF} = GROUND FORCE TORQUE |
| ω_s = SYNCHRONOUS WHEEL SPEED | |
| σ = WHEEL SLIP | |
| μ = EFFECTIVE COEFFICIENT OF FRICTION | |

FIGURE 4. MATHEMATICAL MODEL FOR WHEEL AND TIRE/RUNWAY INTERFACE.

The input to the model is an analog voltage from a D/A converter, with the voltage representing a hydraulic braking pressure command. This pressure command is converted to hydraulic pressure by a pressure servovalve, and applied to the disc brake mechanism. An ideal D/A converter has been assumed. The brake pressure servovalve is approximately ideal, although slew rate (psi/sec) has been taken into consideration. One other notable characteristic, "time to first motion" of the servovalve, has been neglected. This delay time, estimated at 5-10 ms for small signals in a dynamic situation, would manifest itself as an increase in the limit cycling amplitude of the control system. Slew rate of the servovalve has been approximated by adjusting the amount which the counter can increment/decrement per counter service interval. Thus, at the 1000/sec service rate, a count increment of 10 to 25 results in an equivalent slew rate of $10/.001 = 10,000$ psi/sec to $25/.001 = 25,000$ psi/sec. Typical slew rates available in pressure servovalves exceed 50,000 (see Figure 5 below) psi/sec; therefore the system modeled in this thesis is considered conservative in terms of servovalve slew rate performance.

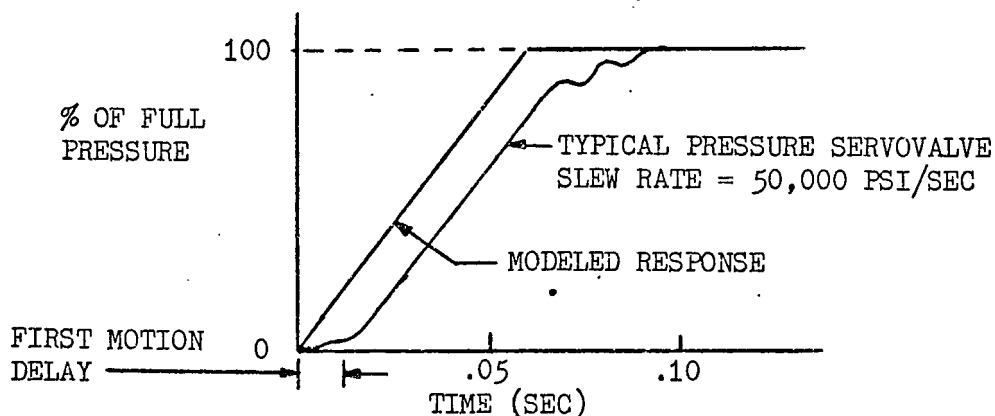


FIGURE 5. TYPICAL PRESSURE SERVOVALVE STEP RESPONSE CHARACTERISTIC FOR 100% COMMAND. (STEP UP OR STEP DOWN)

The brake is modeled by a function generator which converts a hydraulic brake pressure command into a braking torque, T_B . Figure 6 shows the function used, which is based upon the following assumptions:

- A pressure of 500 psi is required to overcome the return spring in the brake mechanism.
- The curve is sized (maximum torque value) such that the brake can overcome a ground force torque of 60,000 ft-lb. This is the torque which would be produced by a tire supporting 80,000 pounds, with a μ of .5, and having a rolling radius of 1.5 foot. Since the maximum weight expected to be supported by one wheel is less than 50,000 pounds, the brake sizing is adequate.
- General shape of the curve is intuitive, with end points based upon the above data assumptions.

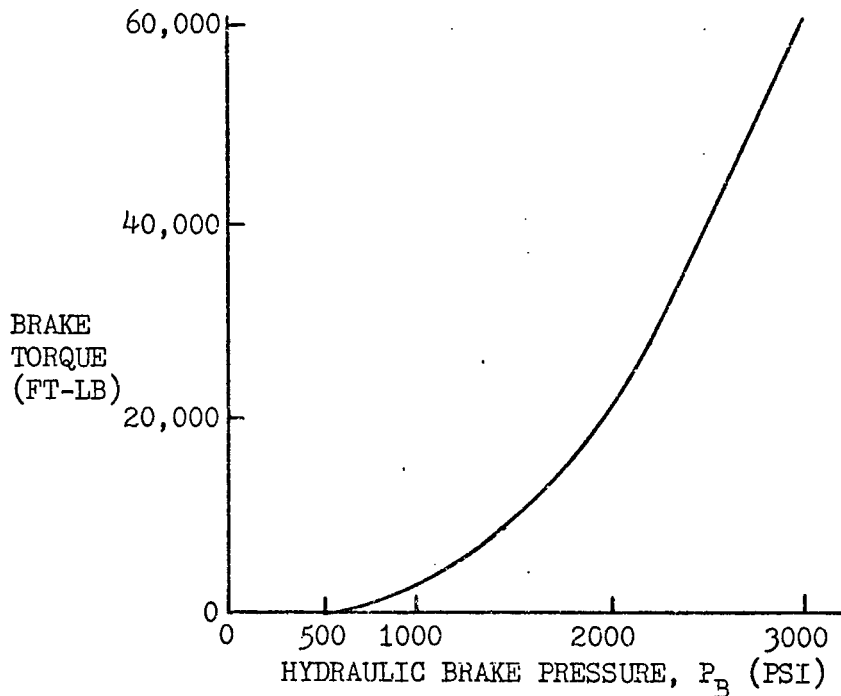


FIGURE 6. BRAKE TORQUE VS BRAKE PRESSURE CURVE.

Acceleration ($\dot{\omega}$) of the wheel is given by:

$$\dot{\omega} = \frac{T_{GF} - T_B}{J_W} \quad (1)$$

where T_{GF} = effective ground force torque

T_B = braking torque

J_W = moment of inertia of the wheel = 23.9 slug-ft²

Wheel speed, ω , is then obtained by integration:

$$\omega = \omega_0 + \int_0^t \dot{\omega} dt \quad (2)$$

Consider next the tire/runway interface as characterized by the mu-slip curve. Mu and slip are defined as follows:

Coefficient of friction, mu (μ). The general definition of coefficient of friction between two surfaces is the ratio of the force required to move (slide) one over the other to the force pressing the two together. For the case of the rolling tire, one of the surfaces (tire) is rotating while the other is stationary (runway). However, if the rotational velocity component at the tire/runway interface does not match the translational velocity component down the runway, then the tire is essentially being dragged along the runway. The force required to drag the tire (which is the braking force) is the product of weight supported by the wheel, and an effective coefficient of friction, mu. This effective mu is the dependent variable in the

mu-slip curve.

Wheel slip, σ . Slip is a measure of the relative velocity between the tire and runway, and is defined by the following equation:

$$\sigma = 1 - \omega/\omega_s \quad (3)$$

Where ω = actual, or measured, tire angular velocity (rad/sec).

ω_s = synchronous velocity, i.e. the angular velocity of a "free-wheeling" tire (rad/sec). This value can be computed from vehicle velocity down the runway if tire rolling radius is known.

Thus using wheel speed from Equation 2 and computed wheel speed a value of slip is determined. The mu-slip curve is then entered, and a corresponding mu value is obtained. The family of curves used in this simulation is shown in Figure 7, representing dry, wet, and icy runway conditions. During simulation test runs, transition from one curve to another is a step function.

Based upon the mu value for a given runway condition and wheel slip, and the weight being supported by the tire (assumed constant), an effective braking force can be determined:

$$F_B = \mu W \quad (4)$$

where W = weight supported by the wheel.

This force, when multiplied by the rolling radius of the tire (r)

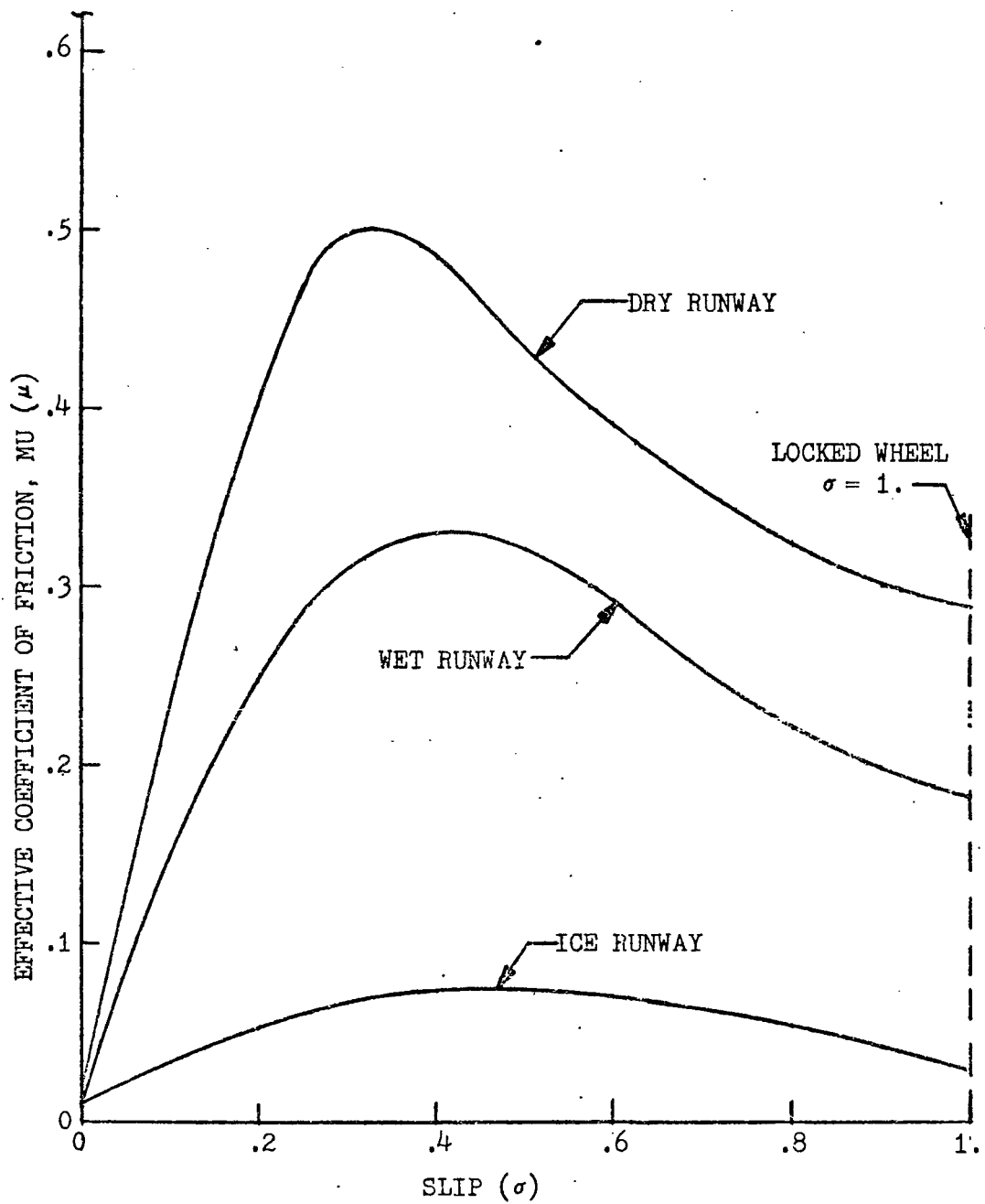


FIGURE 7. A FAMILY OF MU-SLIP CURVES.

produces the resultant ground force torque seen by the braking system.

$$T_{GF} = r F_B \quad (5)$$

Ground force torque T_{GF} is then summed back with the brake torque T_B to close the loop around wheel dynamics.

Ideal torque transducers and wheel speed transducers are assumed. This assumption is considered justified by the fact that strain gauge type torque transducers have frequency response characteristics measured in terms of kilocycles, and wheel speed tachometers (pulse output types) can easily resolve one percent deviations in wheel speed.

2.4 Vehicle Dynamics Math Model

The vehicle dynamics math model has two degrees of translational freedom (X,Y), and one degree of rotational freedom (yaw). A non-elastic structure is assumed. Two coordinate systems are used in the model, designated 'body' and 'landing system.'

Body Coordinate System. This orthogonal system has its origin at the vehicle center of gravity with the $+X_B$ axis directed forward (through the nose) along the flight reference line of the vehicle, and the $+Y_B$ axis directed out the right wing. The $+Z_B$ axis, directed downward, completes the right handed triad.

Landing Coordinate System. This orthogonal system has its origin at the targeted touchdown point on the runway. The X_{LS} and Y_{LS} axes are in the plane of a flat earth (runway surface),

with + X_{LS} axis directed along the center line of the runway in the direction of rollout travel. The + Z_{LS} axis points towards the center of the earth.

Figure 8 indicates the relative alignment of the two coordinate systems.

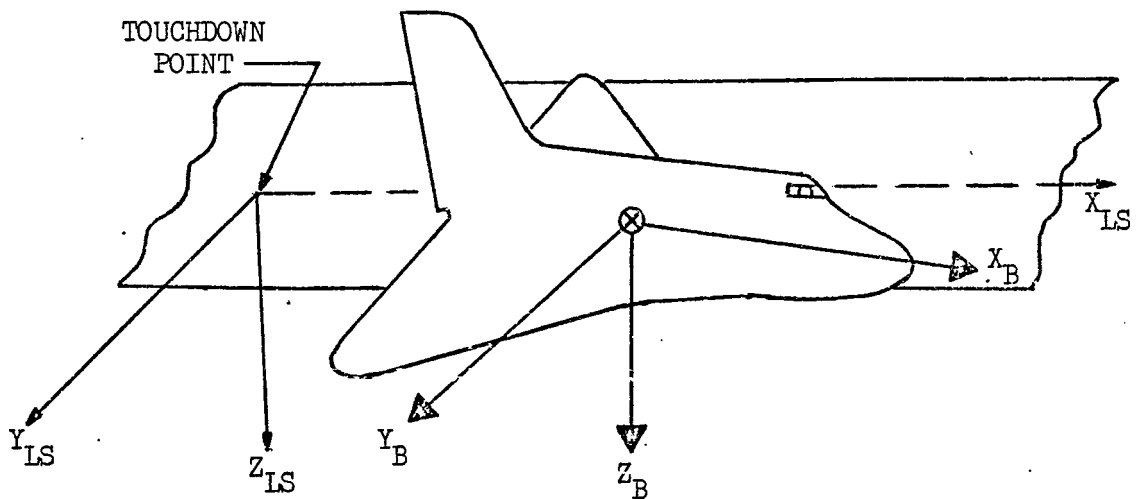


FIGURE 8. RELATIVE ORIENTATION OF LANDING SYSTEM AND BODY AXIS COORDINATE SYSTEMS.

It is assumed that the only forces acting on the vehicle are those caused by braking, aerodynamic drag, and a drag chute. Direction of the net force vector is assumed to be aligned to the X body axis. These assumptions are equivalent to saying that the X_B axis of the vehicle is always aligned with the direction of travel, and that the

vehicle always points directly into the wind (i.e. no cross winds). If a more sophisticated simulation were required, another coordinate system would be used, generally referred to as the aircraft stability axis system. However, the simplified model is adequate to evaluate braking system performance. The assumption that effective Y body axis forces are zero implies that the rolling coefficient of friction of the tires is sufficient to overcome any side sliding forces. Thus the tires are never "scrubbed" across the runway. This assumption could not be made if a detailed study of steering control were being made.

2.5 Vehicle Translational Equations of Motion

Solution of these equations allows tracking of the vehicle center of gravity as it moves down the runway. As indicated in Figure 9, all braking and aerodynamic drag forces act along the X-body axis.

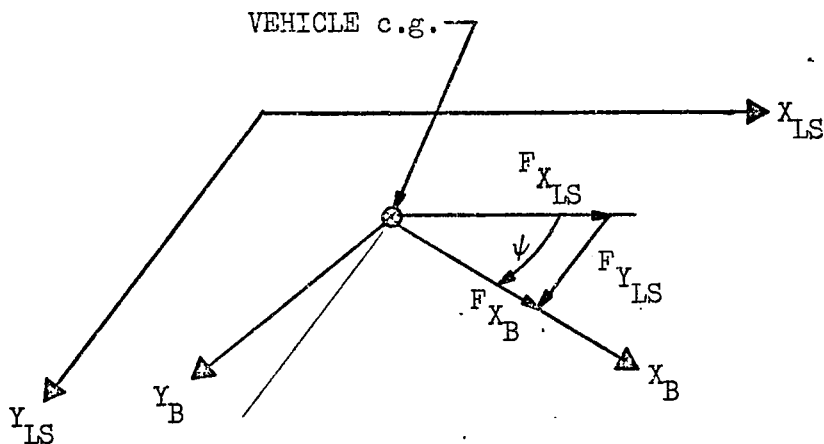


FIGURE 9. RESOLUTION OF BODY FORCES INTO LANDING SYSTEM COORDINATES.

Based upon these forces (F_{XB}), and vehicle mass (M), the vehicle acceleration in terms of body coordinates is computed.

$$\ddot{X}_B = F_{XB}/M \quad (6)$$

Velocity in the body coordinate system is then given by:

$$\dot{X}_B = \dot{X}_B(0) + \int_0^t \ddot{X}_B dt \quad (7)$$

where $X_B(0)$ is the touchdown velocity. Next, velocity components in the landing coordinate system are obtained:

$$\dot{X}_{LS} = \dot{X}_B \cos \psi \quad (8)$$

$$\dot{Y}_{LS} = \dot{X}_B \sin \psi \quad (9)$$

where ψ (yaw) is the angle of rotation between the landing and body coordinate systems. Position in landing system coordinates is obtained by integration of velocity:

$$X_{LS} = X_{LS}(0) + \int_0^t \dot{X}_{LS} dt \quad (10)$$

$$Y_{LS} = Y_{LS}(0) + \int_0^t \dot{Y}_{LS} dt \quad (11)$$

$X_{LS}(0)$ and $Y_{LS}(0)$ are touchdown range and crossrange errors.

Total velocity down the runway is given by:

$$V_T = \left(X_{LS}^2 + Y_{LS}^2 \right)^{\frac{1}{2}} \quad (12)$$

V_T is then used to compute synchronous wheel speed ω_s , which in turn is used to determine wheel slip (see Equation 3). Synchronous wheel speed is given by:

$$\begin{aligned} \omega_s &= V_T \frac{\text{ft}}{\text{sec}} \cdot \frac{\text{rev}}{2\pi r \text{ ft}} \cdot \frac{2\pi \text{ rad}}{\text{rev}} \\ &= \frac{V_T}{r} \frac{\text{rad}}{\text{sec}} \end{aligned} \quad (13)$$

Where r = effective rolling radius of the wheel.

Aerodynamic Drag Force. This force is scaled such that it causes a deceleration of .05 g (approximately 1.6 ft/sec²) at a velocity of 300 ft/sec. It decreases linearly to 0g at zero velocity. Assuming a vehicle mass of 5000 slugs, the force is modeled as shown.

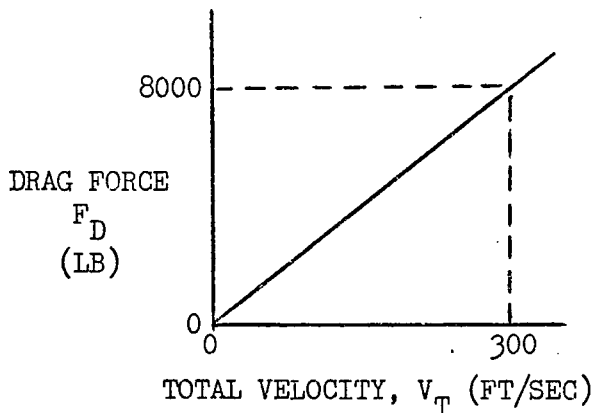


FIGURE 10. AERODYNAMIC DRAG FORCE (F_D) AS A FUNCTION OF TOTAL VELOCITY (V_T).

Drag Chute Force. The drag chute force is represented by a function as shown in Figure 11 below. Scaling is such that, maximum drag chute force at 300 ft/sec velocity is 32,000 lb. General shape of the curve is intuitive.

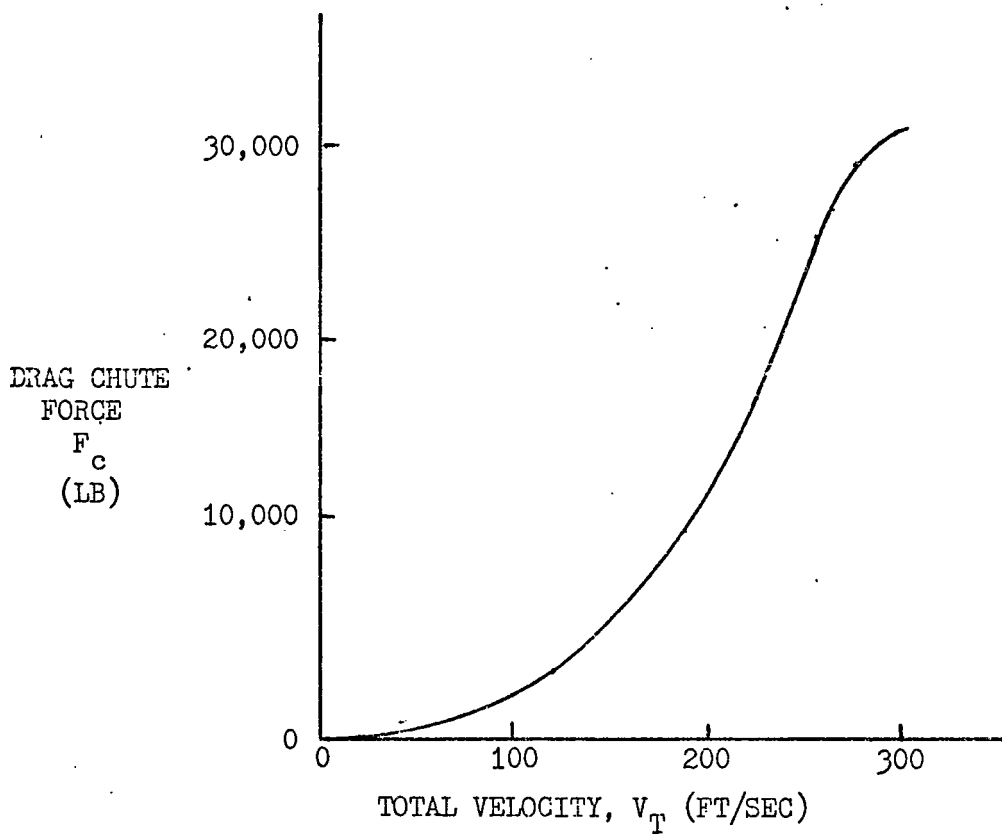


FIGURE 11. DRAG CHUTE EFFECTIVENESS DATA.

2.6 Vehicle Rotational Equations of Motion

The vehicle is assumed to have one degree of rotational freedom, designated yaw (ψ). Thus net torque (T) acting on the vehicle divided by the yaw axis moment of inertia (I_{zz}) determines angular acceleration:

$$\ddot{\psi} = T/I_{zz} \quad (14)$$

where T is in ft-lb, and I_{zz} is in ft-lb-sec². Successive integrations yield angular rate and position.

$$\dot{\psi} = \dot{\psi}(0) + \int_0^t \ddot{\psi} dt \quad (15)$$

$$\psi = \psi(0) + \int_0^t \dot{\psi} dt \quad (16)$$

Note that ψ represents the angle between the body and landing coordinate systems.

Torques acting on the vehicle include the following:

- * Main wheel brake force induced torque. This torque is caused by uneven braking forces of the main landing gear wheels.
- * Nose wheel steering torque.
- * Rudder steering torque.

Torque due to uneven main gear braking is given by:

$$T_B = (F_{BR} - F_{BL}) \cdot L_1 \quad (17)$$

where F_{BR} and F_{BL} are the right and left wheel braking forces, and L_1 is the distance from the vehicle center of gravity to the center-line of either main gear strut. It is assumed that the center of gravity is symmetrically located between the main gear struts.

Rudder torque is modeled as a function of vehicle velocity and rudder position only. Two coefficient-of-rudder-effectiveness curves were prepared, as shown in Figures 12-a and 12-b. These two coefficients, when multiplied by the distance from the center of gravity to the rudder center of pressure (L_4), and a sizing factor, provide the rudder torque term. The sizing factor is 6×10^4 , yielding a torque of near 60,000 ft-lb at a rudder setting of $\approx .75$ radian and 300 ft/sec rollout velocity:

$$T_{RUD} = (C_{RUD-1}) \cdot (C_{RUD-2}) \cdot L_4 \cdot 6 \times 10^4 \quad (18)$$

Nosewheel steering torque is a function of the effective coefficient of friction of the nosewheel (μ_{NW}), weight on the nosewheel (W_{NW}), and distance between the vehicle center of gravity and the nosewheel strut (L_3). The coefficient of friction curve (a function of nosewheel angle) is given in Figure 13. Nosewheel steering torque

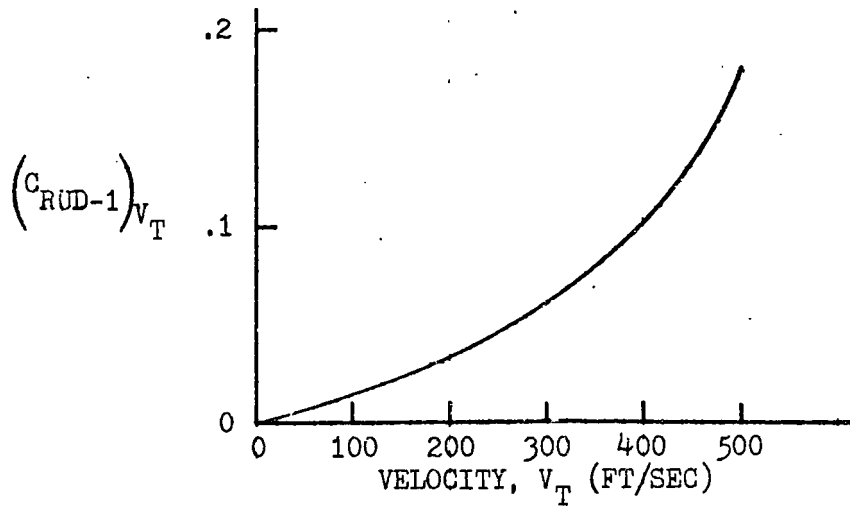


FIGURE 12-a. RUDDER TORQUE EFFECTIVENESS AS A FUNCTION OF VELOCITY.

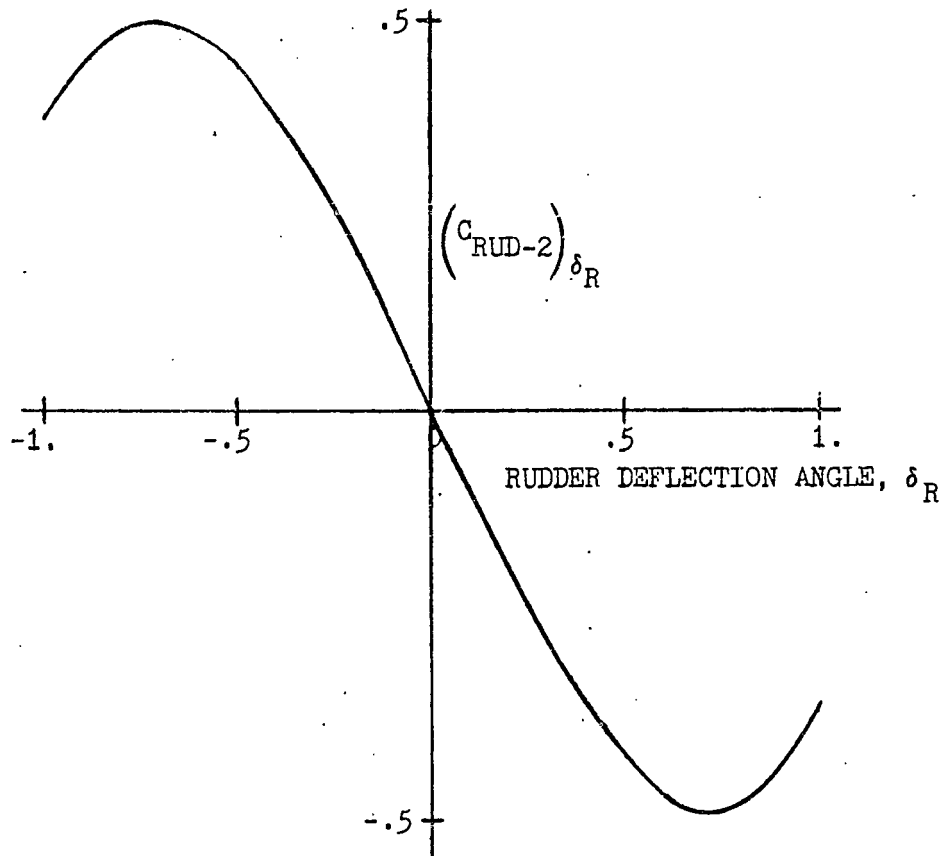


FIGURE 12-b. RUDDER TORQUE EFFECTIVENESS AS A FUNCTION OF RUDDER POSITION.

is obtained by the following equation:

$$T_{NW} = W_{NW} \cdot \mu_{NW} \cdot L_3 \quad (19)$$

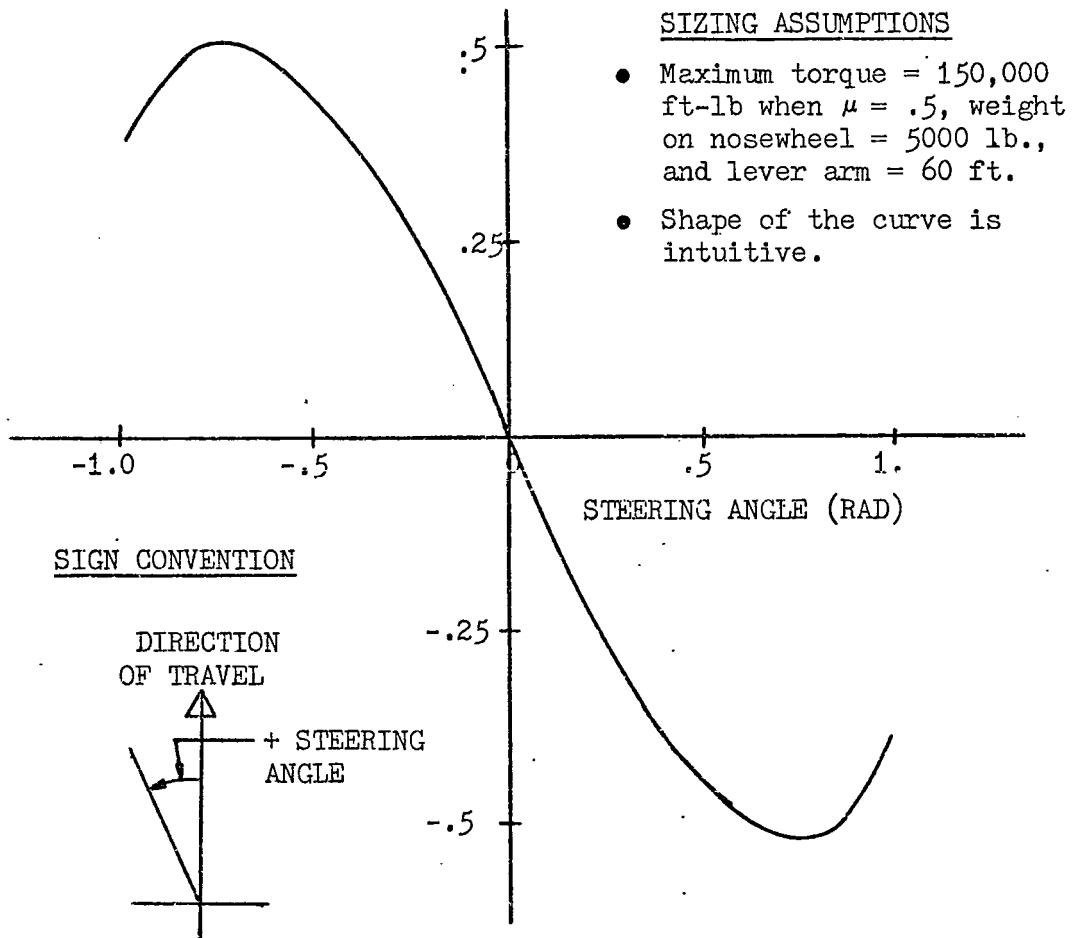


FIGURE 13. NOSEWHEEL COEFFICIENT OF FRICTION AS A FUNCTION OF STEERING ANGLE.

2.7 Digital Computer Simulation and CSMP. (6)

The mathematical models were implemented in an all digital simulation, using FORTRAN and CSMP languages. CSMP is an applications oriented input language which accepts problems expressed in the form of either analog block diagram or systems of differential equations. It eliminates the requirement for writing FORTRAN subprograms for such functions as integration, function generation, limiters, data plotting, and data printout formatting. A variety of integration techniques are available (trapezoidal, Adams, Runge-Kutta, Milne, etc.), with integration step size either fixed or variable.* Some of the mathematical functions used in the program are indicated in Table 1. Simplified flow diagrams for the wheel/runway interface and the vehicle math models are given in Figures 14 and 15.

In order to conserve computer run time, all segments of the program are not executed during each pass (.0001 second). Vehicle equations of motion are solved every 50 milliseconds and the counter output is serviced once per millisecond. Only wheel rotation dynamics are solved each pass. Two integration methods were used for various runs: Adams and Simpsons.

* Adams Method.

$$Y_{t + \Delta t} = Y_t + \frac{\Delta t}{2} (3\dot{Y}_t - \dot{Y}_{t - \Delta t}) \quad (20)$$

*variable step size not available for all integration techniques.

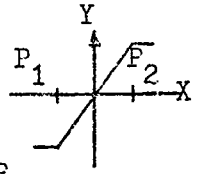
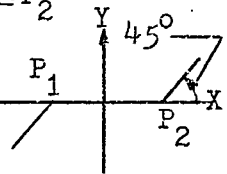
GENERAL FORM	FUNCTION
<p>Y = AFGEN (FUNCT, X)</p> <p>ARBITRARY FUNCTION GENERATOR</p> <p>(LINEAR INTERPOLATION)</p>	<p>Y = FUNCT (X)</p>
<p>Y = NLFGEN (FUNCT, X)</p> <p>ARBITRARY FUNCTION GENERATOR</p> <p>(QUADRATIC INTERPOLATION)</p>	<p>Y = FUNCT (X) $x_0 \leq x \leq x_n$</p>
<p>Y = LIMIT (P₁, P₂, X)</p> <p>LIMITER</p>	<p>Y = P₁ X < P₁</p> <p>Y = P₂ X > P₂</p> <p>Y = X P₁ ≤ X ≤ P₂</p> 
<p>Y = DEADSP (P₁, P₂, X)</p> <p>DEAD SPACE</p>	<p>Y = 0 P₁ ≤ X ≤ P₂</p> <p>Y = X - P₂ X > P₂</p> <p>Y = X - P₁ X < P₁</p> 
<p>Y = INTGRL (IC, X)</p> <p>Y (0) = IC</p> <p>INTEGRATOR</p>	<p>Y = ∫₀^t X dt + IC</p> <p>EQUIVALENT LAPLACE TRANSFORM: $\frac{1}{S}$</p>

TABLE 1. PARTIAL LISTING OF SPECIAL CSMP FUNCTIONS

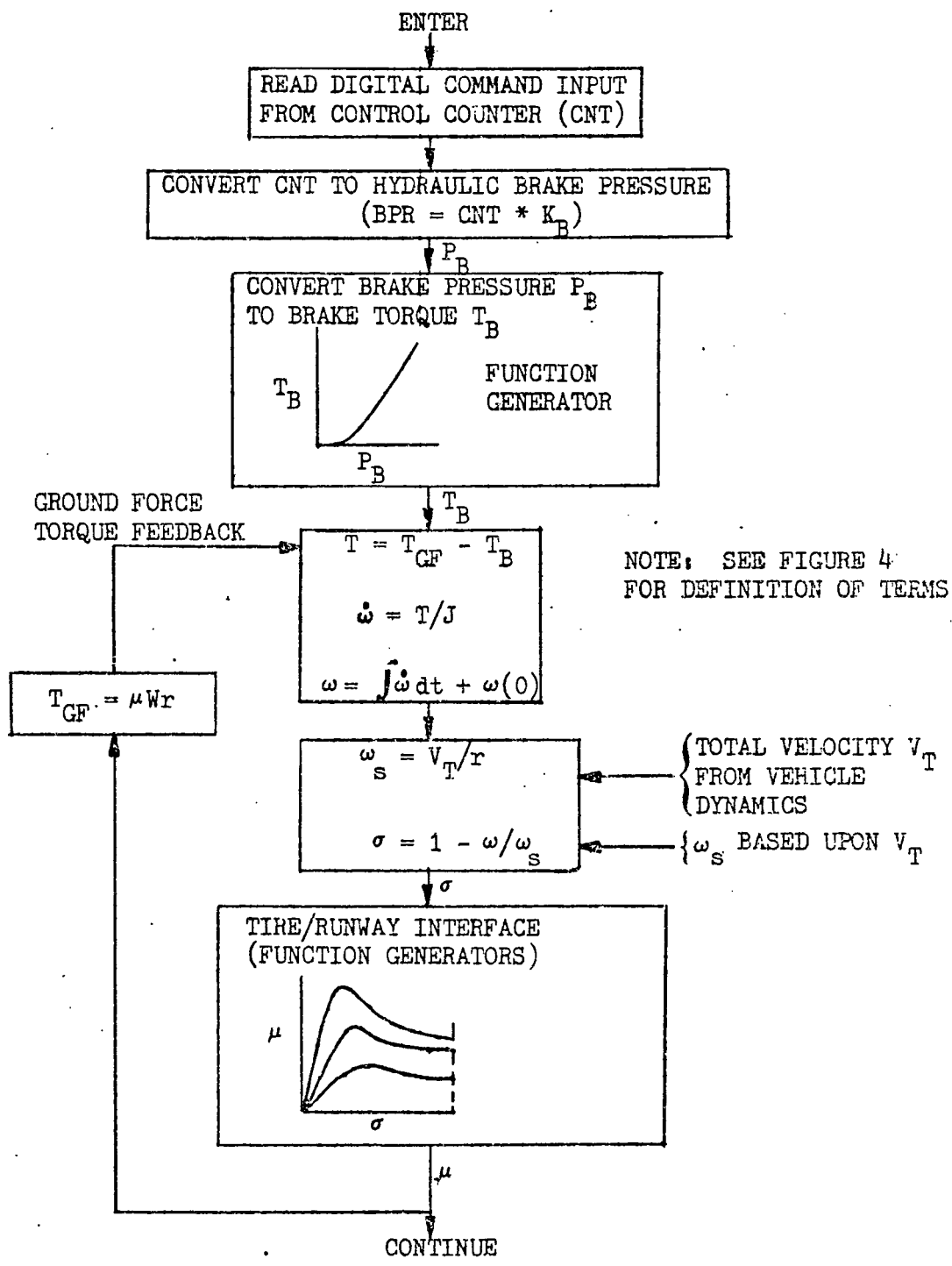


FIGURE 14. SIMPLIFIED SOFTWARE FLOW DIAGRAM FOR WHEEL DYNAMICS AND WHEEL/RUNWAY INTERFACE MODEL.

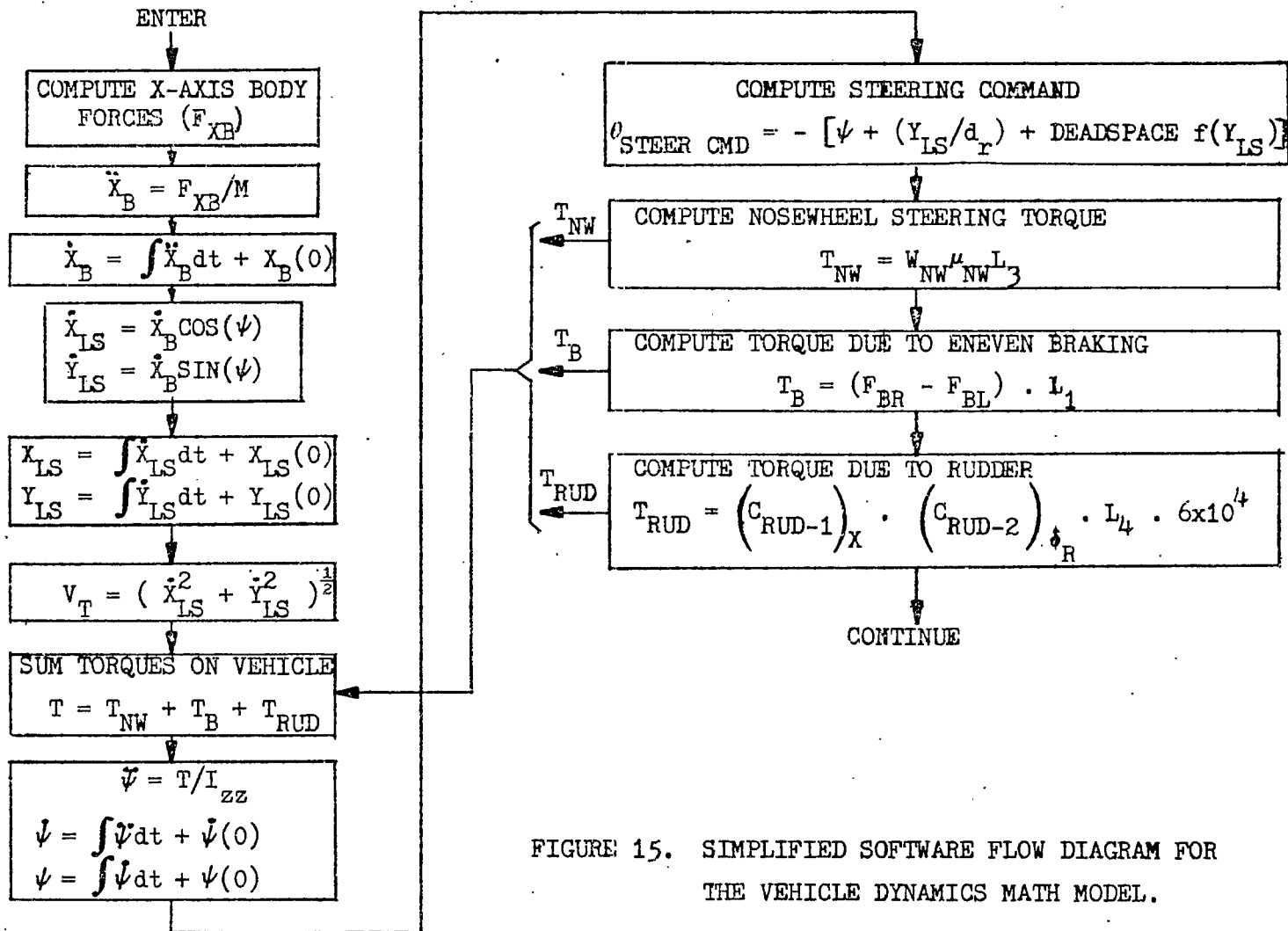


FIGURE 15. SIMPLIFIED SOFTWARE FLOW DIAGRAM FOR THE VEHICLE DYNAMICS MATH MODEL.

- Simpsons Rule Method.

$$\text{Predictor: } Y_t^p + \frac{\Delta t}{2} = Y_t + \frac{\Delta t}{2} X_t \quad (21)$$

$$Y_t^p + \Delta t = Y_t^p + \frac{\Delta t}{2} + \frac{\Delta t}{2} X_t + \frac{\Delta t}{2} \quad (22)$$

$$\text{Corrector: } Y_t^c + \Delta t = Y_t + \frac{\Delta t}{6} (X_t + 4X_t + \frac{\Delta t}{2} + X_t + \Delta t) \quad (23)$$

Only slight (less than .5%) differences in output data were observable when comparing the two methods. These methods were chosen primarily for their simplicity, and hence speed. Even with these fast integration routines, an average of 12.5 minutes of computer run time was required to simulate 5 to 10 seconds of real time.

Several features were incorporated into the program to allow control system configuration and mode changes during run time.

CHAPTER 3

DESIGN OF AN AUTOMATIC ANTISKID BRAKING CONTROL SYSTEM

3.1 Design Approaches and the Friction-Slip Curve

As indicated in Chapter 1, design of an antiskid braking control system must take into consideration the characteristic μ -slip curve. Examination of the curve suggests several possible design approaches for automatic braking systems, each distinguishable by the desired parameter to be controlled. Four feasible schemes are discussed below. The area of control for each scheme is indicated in Figure 16.

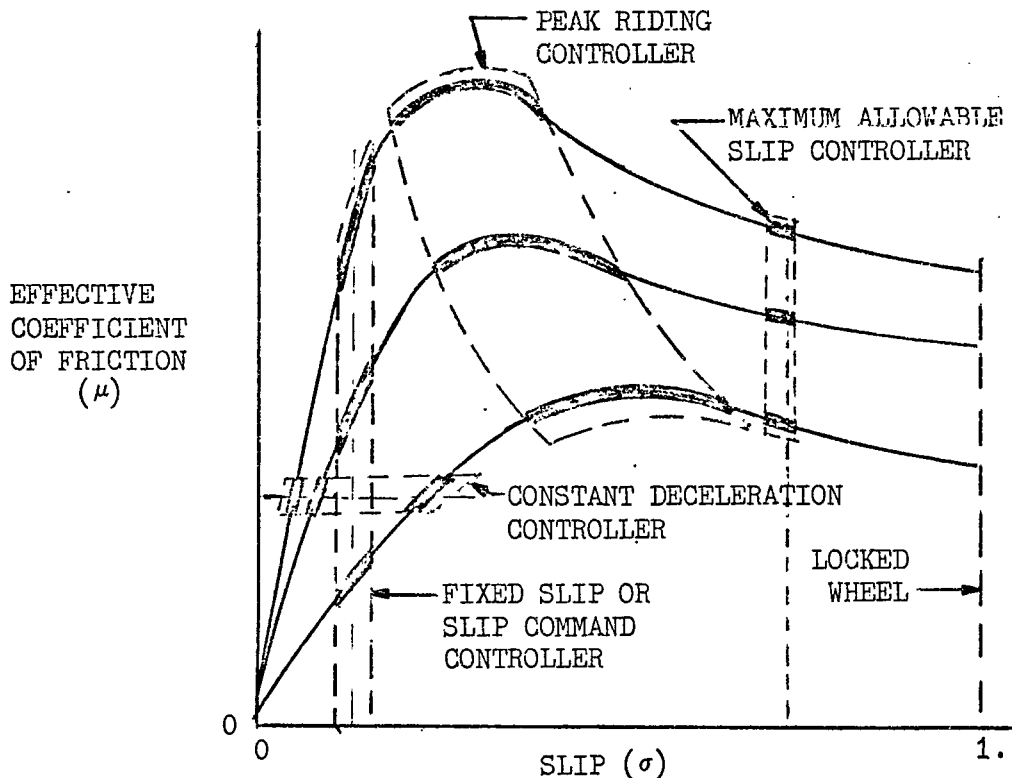


FIGURE 16. AREAS OF CONTROL FOR VARIOUS CONTROL SCHEMES

Peak Riding Controller. This controller maintains braking control around the peak of the μ -slip curve. It is the most efficient controller in terms of stopping distance (stops in shortest distance). As a point of interest, continuous control about the peak can possibly result in an undesirably high degree of tire wear. Resolution of this possibility is beyond the scope of this thesis, however, since actual hardware experimentation would be required.

The fundamental problem encountered in implementing this scheme is sensing the peak of the μ -slip curve. Although slip can be determined in a relatively straightforward manner (Equation 3), there is no simple means for measuring the coefficient of friction (μ). A scheme for sensing this peak is developed later in this Chapter.

The peak riding controller is considered the most logical antiskid backup for pilots manual braking.

Slip Command Controller. As shown in Figure 16, this control scheme operates about some predetermined or commanded slip value, and only requires measurement of wheel speed and vehicle velocity for implementation. The slip value can be pilot selected, or can be automatically controlled by a braking law.

Inspection of the characteristic μ -slip curve indicates that, for values of slip between zero and the peak μ point, an increase in slip can be equated to an increase in braking, and vice versa. This slip-to-braking relationship is the basis for the slip command controller.

Note that this system does not attempt to achieve maximum braking effectiveness. Also, the slip command controller requires a backup antiskid system.

Constant Vehicle Deceleration Controller. This system would attempt to maintain vehicle deceleration at some fixed value by adjusting hydraulic brake pressure. The commanded deceleration value could be computed by a control law which attempts to stop the vehicle within a specified distance. Such a system would be susceptible to skid should large decelerations be required; thus it would require a backup antiskid system.

Combination. The braking system developed in this thesis is actually a combination of the above three schemes, and can function in two modes: 1. Totally automatic braking with antiskid protection, or 2. Antiskid protection system only which monitors wheel behavior and simply prevents wheel skid should the pilot apply excessive brake pressure.

3.2 An Automatic Antiskid Braking Control System: Functional Description.

An automatic antiskid braking control system was designed which implements the "combination" scheme outlined above. The central feature of the control system is an up/down counter whose count is ultimately converted into hydraulic braking pressure. The various control functions are realized by controlling the count rate and direction (up, down) of this counter. There is one counter per braked wheel.

Basic elements of the braking control system are shown in Figure 17. Functions and/or mathematical derivations associated with each component (software routine, or hardware) are discussed next.

3.3 Slip Command Controller with Rollout Estimator.

This braking control scheme incorporates a rollout estimator routine which computes a 'reference trajectory' aimed at stopping the vehicle within 6000 feet. Braking control is implemented by means of a slip command controller. This controller operates on rollout distance error obtained from the rollout estimator; if estimated rollout distance exceeds 6000 feet, additional wheel slip is commanded, and conversely, if estimated rollout distance is less than 6000 feet the wheel slip command is reduced. Thus, as long as commanded slip does not exceed that value associated with the peak of the mu-slip curve, the slip command is directly proportional to braking force.

Initialization of the system occurs when the first squat (strut compressed) switch is energized. Once engaged, the estimator continues to operate until the aircraft stops. Thus if the aircraft should momentarily lift from the runway the rollout estimator does not disengage.

Deceleration ($-\ddot{X}$) along the X axis of the landing coordinate system (i.e. along runway centerline) is the only input required by the rollout estimator. This signal is available directly from the accelerometers mounted on the stable platform of the Inertial Measurement Unit (IMU). Deceleration is successively integrated to obtain velocity (\dot{X}) and elapsed rollout distance (d_e). The rollout

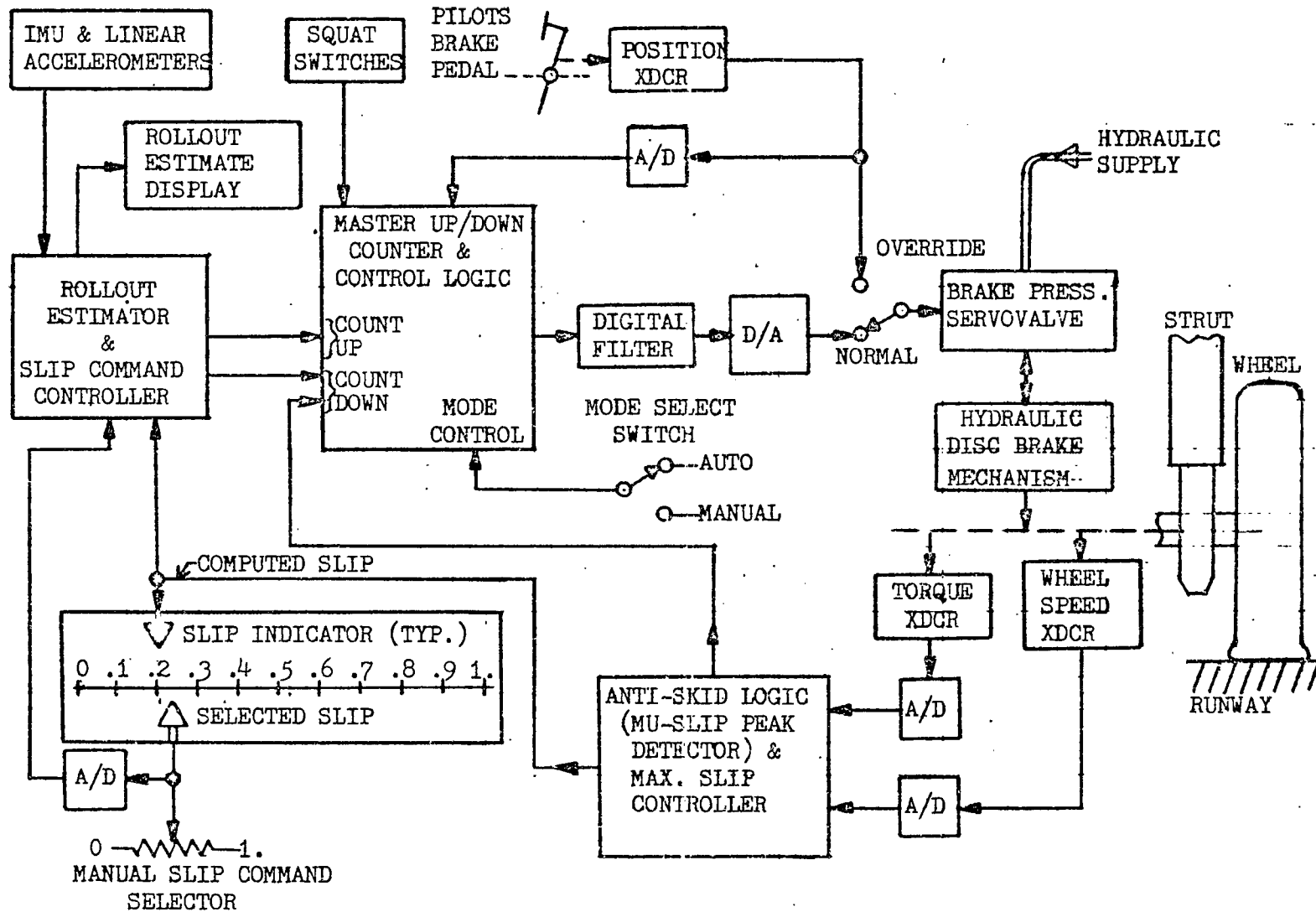


FIGURE 17. FUNCTIONAL BLOCK DIAGRAM OF AUTOMATIC ANTISKID BRAKING CONTROL SYSTEM.

estimator functions as follows:

\ddot{X} is read at a relatively high sampling rate and averaged over a fixed period of time (say .05 sec.). It is then numerically integrated to determine velocity, \dot{X} ;

$$\dot{X} = \int_0^t \ddot{X} dt + X(0) \quad (24)$$

Note that X will always be negative (deceleration) since the shuttle is unpowered during landing and rollout. Average deceleration and velocity are used to compute estimated time remaining until the vehicle stops. This estimate presumes continued constant deceleration at the averaged value (see Figure 18).

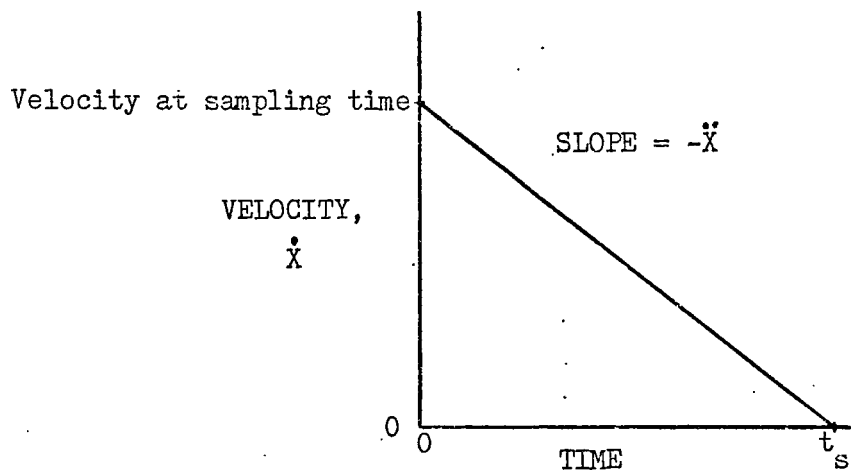


FIGURE 18. ROLLOUT ESTIMATOR PARAMETERS.

Letting $\ddot{X}(t)$ and $\dot{X}(t)$ represent acceleration and velocity at time t , compute time to stop (t_s) as:

$$t_s = \dot{X}(t) / \ddot{X}(t) \text{ sec.} \quad (25)$$

Then, remaining rollout distance (d_r) is determined by:

$$d_r = .5 \ddot{x} t_s^2 \quad (26)$$

The braking control law thus becomes:

If $d_e + d_r > 6000$ ft, increase slip cmd by $\Delta\sigma_c$

If $d_e + d_r = 6000$ ft, leave slip cmd at last value

If $d_e + d_r < 6000$ ft, decrease slip cmd by $\Delta\sigma_c$

where d_e is the elapsed rollout distance from touchdown, and $\Delta\sigma_c$ is computed as follows:

$$\Delta\sigma_c = \frac{d_e + d_r - 6000}{6000} \quad (27)$$

$\Delta\sigma_c$ is then limited to a maximum increment of .05 to .1 to prevent unnecessarily large braking transients.

The same slip command is sent out to all four wheel braking control systems. And, under normal runway landing conditions (dry, consistent runway material) this control scheme will bring the vehicle to a smooth stop while operating to the left of the peak of the mu-slip curve.

Figure 19 shows the software flow diagram for this braking scheme.

3.4 Brake Pressure Up/Down Counter and Counter Control Logic

There is one UP/DOWN counter per braked wheel. The number stored in this counter is ultimately converted to hydraulic brake pressure via a D/A converter and closed loop pressure servo. For purposes of this thesis, bit weighting for the counter is 1.0 psi per bit, and the counter services its control inputs 100 times per second. All count control logic is accomplished via a software routine as shown in Figure 20. However, for convenience of representation, the control

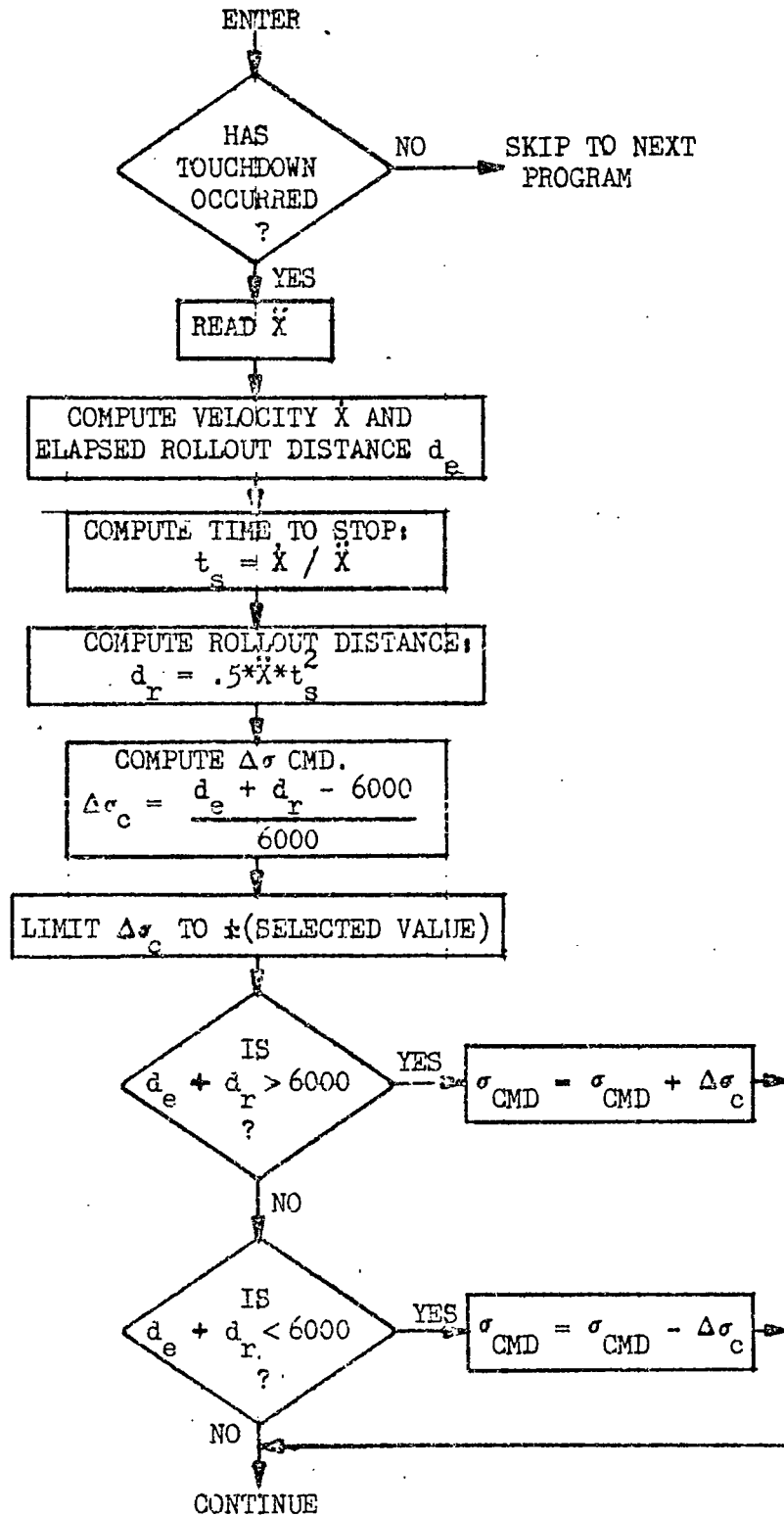


FIGURE 19. FLOW DIAGRAM FOR ROLLOUT ESTIMATOR AND SLIP COMMAND CONTROLLER.

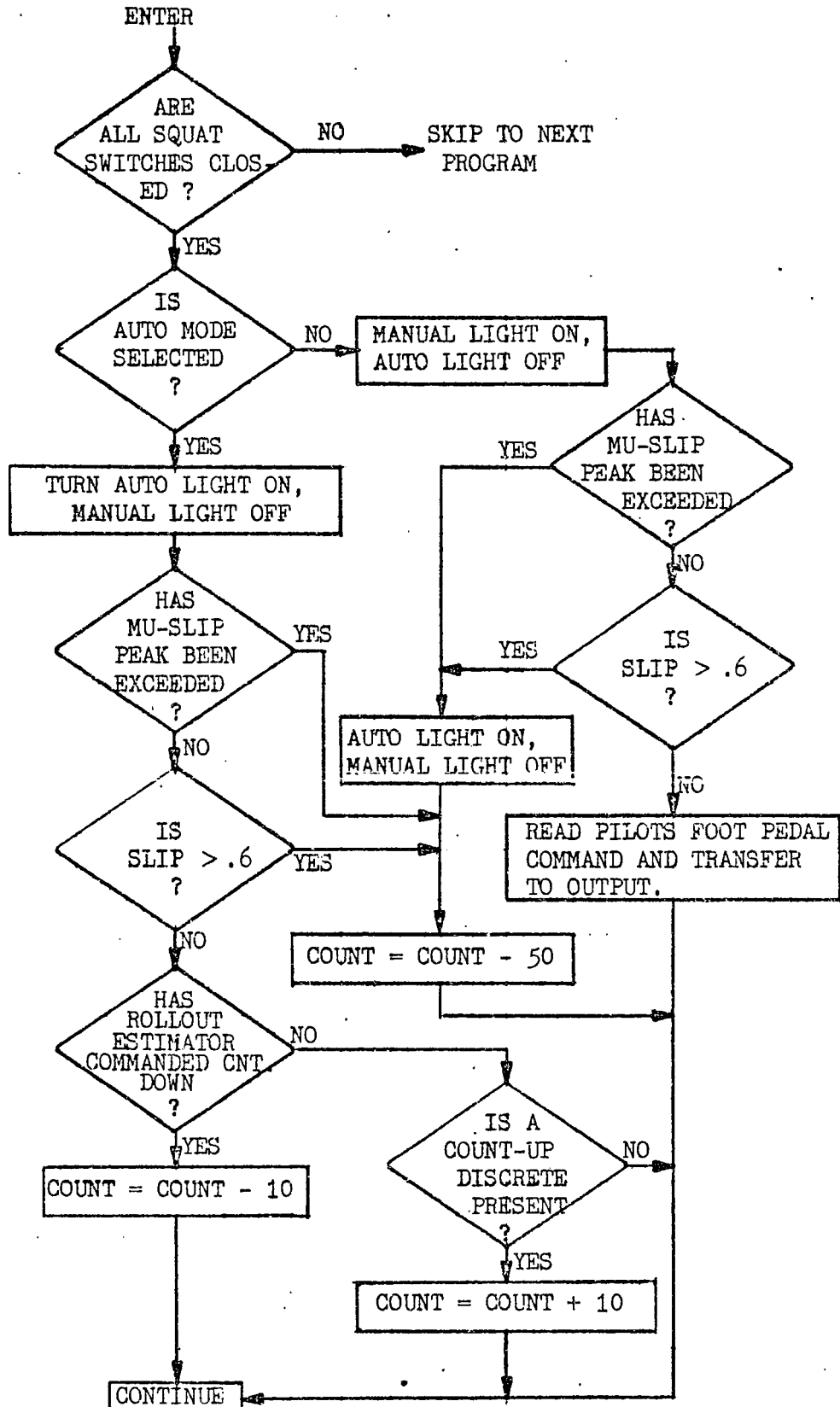


FIGURE 20. MASTER UP/DOWN COUNTER SOFTWARE FLOW DIAGRAM.

logic, counter, and count storage functions are indicated in terms of AND and OR gates, storage registers, and switches as shown in Figure 21. The following functional description is based upon that Figure.

Outputs of the UP/DOWN counter and Final Output Register are set and held at zero until a logical "1" is received from the squat switch monitor. These squat switches are located in the landing gear struts, and are energized as the struts compress under aircraft weight. Thus, braking cannot be initiated until all main landing gear wheels and the nose gear wheels are on the ground, i.e. the squat monitor requires that all three struts be compressed simultaneously before issuing the braking enable discrete.

Next, the MANUAL/AUTOMATIC switch function is checked to see which operating mode has been selected by the pilot. Note that the MANUAL mode switch position is overridden (i.e. control reverts to completely automatic operation) if the antiskid system senses that the peak of the mu-slip curve has been exceeded, or that wheel slip is exceeding the maximum allowable value. First, for sake of discussion, assume that the MANUAL mode has been pilot selected and has not been overridden. The pilot's foot pedal position is sensed by a linear position transducer and converted into a digital word. Scaling of the transducer and A/D converter is such that zero deflection of the brake pedal produces a count of zero, and full deflection produces a count of 3000 (equivalent to 3000 psi brake pressure). This count is transferred directly to the Final Output Register via AND gates A1 through

A13, and thirteen OR gates. Thus, within limits of the antiskid protection system, the pilot is in control of braking.

Next, assume that the AUTOMATIC mode has been selected. If it is selected prior to touchdown, then the UP/DOWN Counter will have a zero count stored prior to being released by the squat switch monitor. (Otherwise, the UP/DOWN Counter simply monitors and tracks the output of the Final Output Register, and is therefore ready to assume control smoothly.) The Counter counts up at each service interval provided there is a count-up logic discrete from the slip command controller, and no count-down discrettes are present. Counting up will continue at a preselected rate as long as this logic is satisfied. However, presuming an adequate braking system (i.e. one capable of locking the wheels at something less than full pressure) it is unlikely that full count will be achieved before one of the count-down logical variables becomes true (logical 1). When any of the count-down discrettes are present, the count-up discrete is inhibited. Counting down will continue until the count-up logic is again satisfied. Thus limit cycling about some fixed count will result under steady state (constant runway) conditions. Limit cycle amplitude will be determined by the increment/decrement value and the counter service rate.

Next, assume that either maximum allowable slip or the peak of the mu-slip curve is exceeded. If not already selected, the mode control discrete is set to AUTO and the Counter begins counting down at maximum rate until the offending condition is removed. A maximum

count rate of 50,000 per second was selected, approximating a typical slew rate (50,000 psi/sec) achievable by currently operational pressure control servovalves.

As indicated in the counter routine flow diagram in Figure 20, various discrettes within the control logic are monitored and displayed in the cockpit.

3.5 Digital Filter

The output count of the UP/DOWN Counter will behave approximately as a sine wave during steady state limit cycle operation. If the limit cycle frequency is in the range of 10 to 20 Hz and sufficient energy is available, there is a danger of exciting structural resonance of the landing gear. Therefore, it is desirable to incorporate a low pass filter at some point between the output of the counter and the input to the brake pressure control servovalve. Two choices are apparent (see Figure 17).

- Digital filter at the output of the UP/DOWN Counter.
- Continuous filter on the output of the D/A Converter.

The digital filter approach is investigated in this thesis.

The basis filter requirement is shown in the following gain-vs-frequency diagram. It is intended that the filter only accomplish simple smoothing and attenuation of high frequency brake pressure commands.

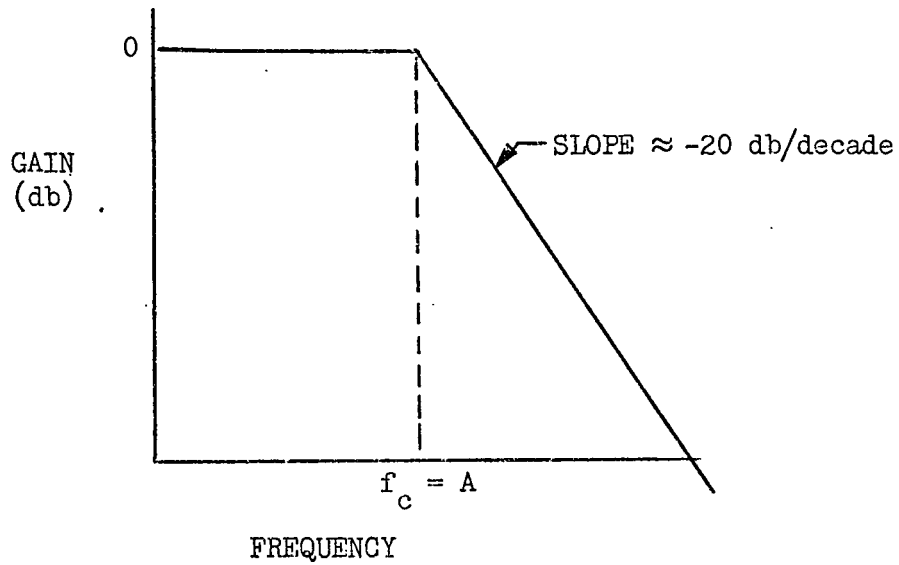


FIGURE 22. GAIN-VS-FREQUENCY CURVE FOR $A/(S+A)$ TRANSFER FUNCTION

Realization of this filter is accomplished via Z transformation of an equivalent S domain filter. Consider the system shown in Figure 23.

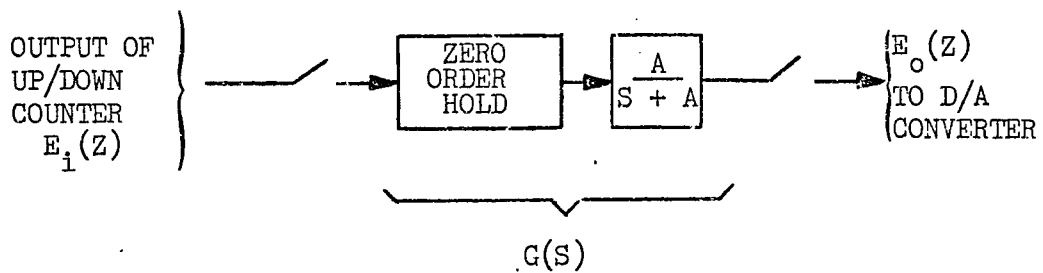


FIGURE 23. S DOMAIN REPRESENTATION OF DIGITAL FILTER

The S domain transfer function for the zero order hold is:

$$\mathcal{L}[\text{Zero Order Hold}] = \frac{1 - e^{-ST}}{S} \quad (28)$$

Therefore:

$$\begin{aligned} G(S) &= \frac{1 - e^{-ST}}{S} \cdot \frac{A}{S + A} \quad (29) \\ &= (1 - e^{-ST}) \cdot \left[\frac{A}{S(S + A)} \right] \end{aligned}$$

Partial fraction expansion yields:

$$G(S) = (1 - e^{-ST}) \cdot \left[\frac{K_1}{S} + \frac{K_2}{S + A} \right] \quad (30)$$

Evaluating K_1 and K_2 :

$$K_1 = \frac{A}{S + A} \Big|_{S=0} = 1$$

$$K_2 = \frac{A}{S} \Big|_{S=-A} = -1$$

Thus;

$$G(S) = (1 - e^{-ST}) \left[\frac{1}{S} - \frac{1}{S + A} \right] \quad (31)$$

Now, from Z transform tables⁽⁷⁾ obtain:

$$Z \left[\frac{1}{S} \right] = \frac{Z}{Z - 1} \quad (32)$$

$$Z \left[\frac{1}{S + A} \right] = \frac{Z}{Z - e^{-AT}} \quad (33)$$

And, since $Z = e^{ST}$, $G(Z)$ can now be written:

$$G(Z) = (1 - Z^{-1}) \cdot \left[\frac{Z}{Z-1} - \frac{Z}{z - e^{-AT}} \right] = \frac{1 - e^{-AT}}{Z - e^{-AT}} \quad (34)$$

Mechanization of this filter requires an expression in terms of Z^{-1} . Thus dividing numerator and denominator by Z yields:

$$G(Z) = \frac{(1 - e^{-AT})/Z}{(Z - e^{-AT})/Z} = \frac{(1 - e^{-AT})Z^{-1}}{1 - Z^{-1}e^{-AT}} = \frac{E_o(Z)}{E_i(Z)} \quad (35)$$

Cross multiplying:

$$E_o(Z) - e^{-AT}Z^{-1}E_o(Z) = (1 - e^{-AT})Z^{-1}E_i(Z) \quad (36)$$

Finally:

$$E_o(Z) = e^{-AT}Z^{-1}E_o(Z) + (1 - e^{-AT})Z^{-1}E_i(Z) \quad (37)$$

Figure 24 indicates the block diagram representation for equation 37.

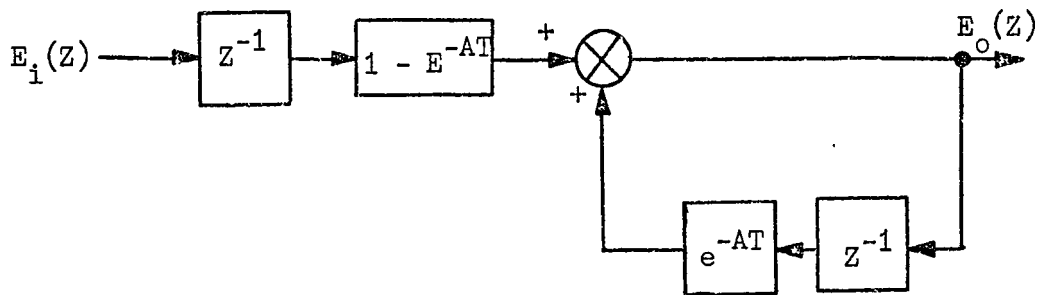


FIGURE 24. BLOCK DIAGRAM FOR FIRST ORDER LAG DIGITAL FILTER.

Values of e^{-AT} and $(1 - e^{-AT})$ corresponding to selected values of A and T are given in Table 2. Some typical response curves for the filter are shown in Figures 25 and 26.

	FREQ (HZ)	FREQ (RAD/SEC)	e^{-AT}	$1-e^{-AT}$
T = .0010	.100	.628	.9994	.0006
	.200	1.257	.9987	.0013
	.500	3.142	.9969	.0031
	1.000	6.283	.9937	.0063
	2.000	12.566	.9875	.0125
	5.000	31.416	.9690	.0310
	10.000	62.832	.9391	.0609
	20.000	125.664	.8819	.1181
	50.000	314.159	.7304	.2696
	100.000	628.319	.5335	.4665
T = .0100	.100	.628	.9937	.0063
	.200	1.257	.9875	.0125
	.500	3.142	.9690	.0310
	1.000	6.283	.9391	.0609
	2.000	12.566	.8819	.1181
	5.000	31.416	.7304	.2696
	10.000	62.832	.5335	.4665
	20.000	125.664	.2846	.7154
	50.000	314.159	.0432	.9568
	100.000	628.319	.0019	.9981
T = .10000	.100	.628	.9391	.0609
	.200	1.257	.8819	.1181
	.500	3.142	.7304	.2696
	1.000	6.283	.5335	.4665
	2.000	12.566	.2846	.7154
	5.000	31.416	.0432	.9568
	10.000	62.832	.0019	.9981
	20.000	125.664	.0000	1.0000
	50.000	314.159	.0000	1.0000
	100.000	628.319	.0000	1.0000

TABLE 2. COEFFICIENT DATA FOR A FIRST ORDER DIGITAL FILTER.

3.6 D/A Converter

The number stored in the Brake Pressure UP/DOWN Counter must be converted to an analog voltage to drive the brake pressure servo-valve. This is accomplished via a D/A converter, which has a resolution of 1 psi/bit. There is one D/A converter per braked wheel.

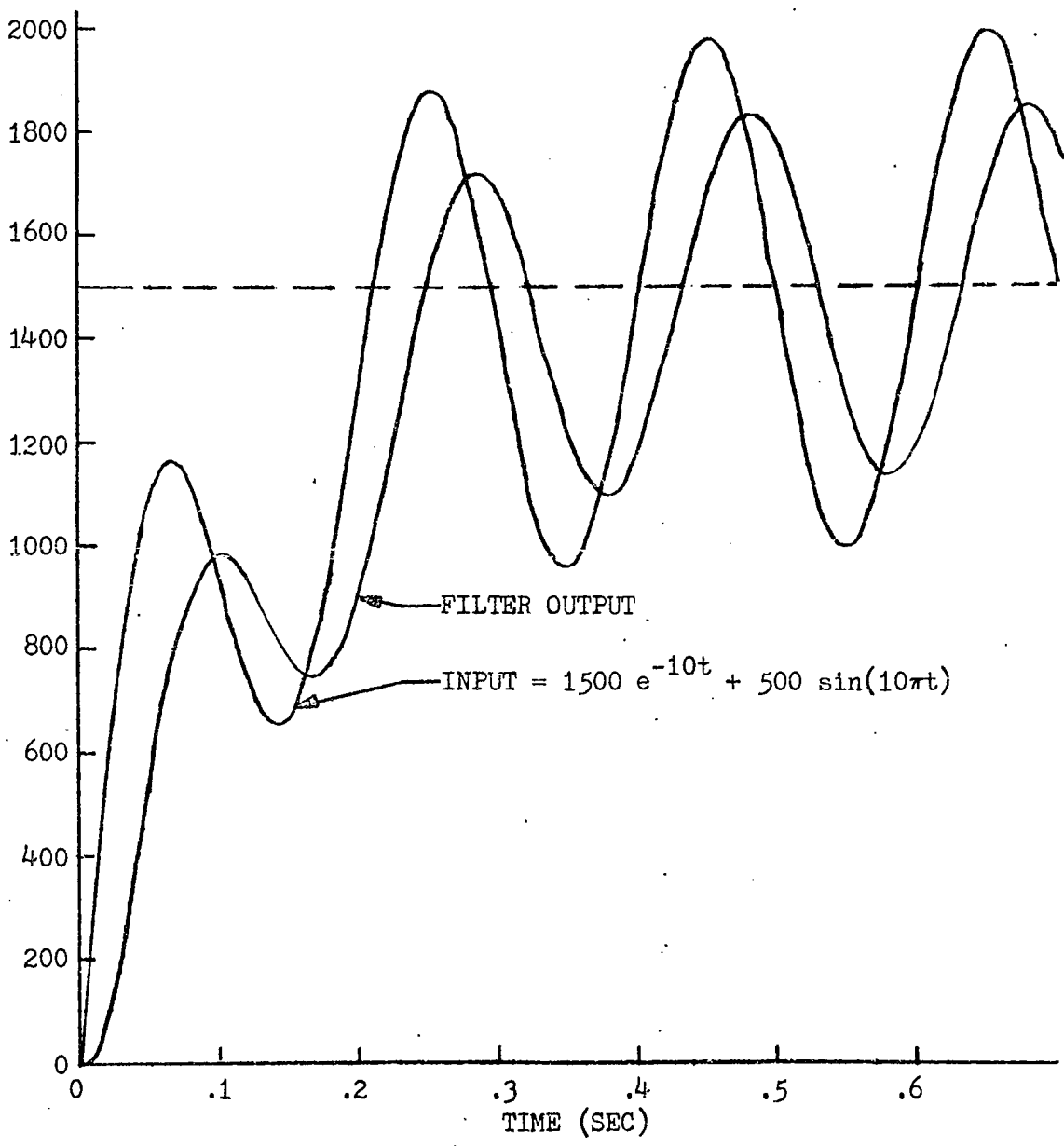
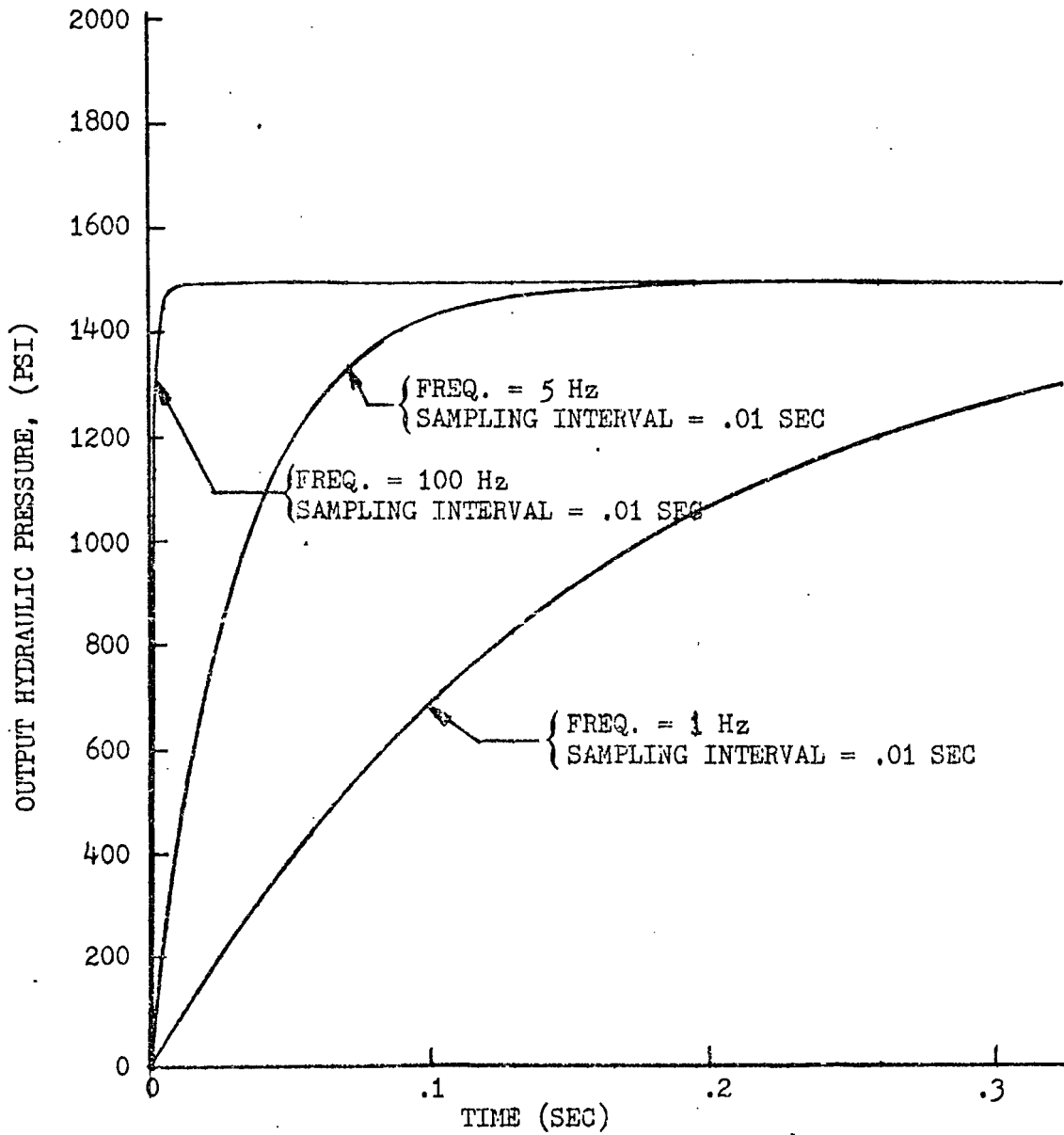


FIGURE 25. RESPONSE OF DIGITAL FILTER TO EXPONENTIAL + 5 Hz SINUSOID.



NOTE: A STEP INPUT OF 1500 PSI IS APPLIED TO THE FILTER AT TIME 0.

FIGURE 26. TYPICAL RESPONSE OF A FIRST ORDER DIGITAL FILTER TO STEP INPUT.

3.7 Brake Pressure Control Valve

This is a pressure control servovalve which, by means of pressure feedback, converts an analog input voltage into hydraulic pressure.

Functionally, the servovalve can be represented as shown below:

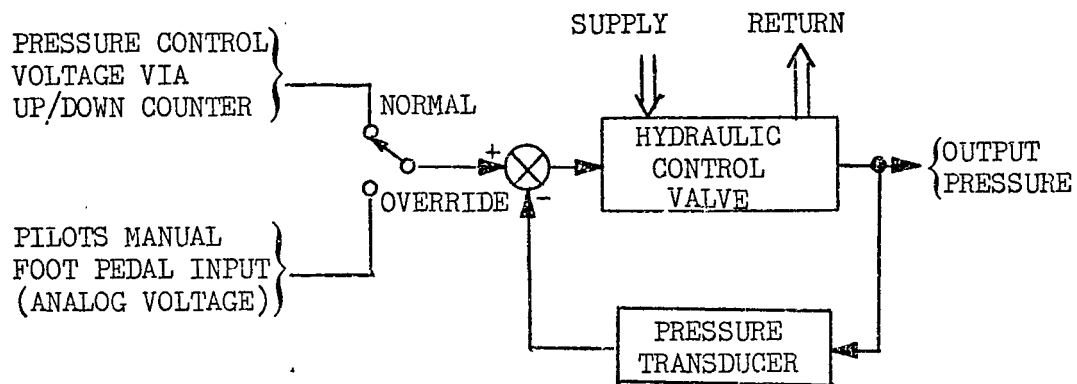


FIGURE 27. BRAKE PRESSURE CONTROL VALVE BLOCK DIAGRAM

Note that, in the event of a failure in the automatic control system, brake pressure commands can be applied directly to the servovalve input from the pilots brake pedal. This OVERRIDE mode is considered a "last resort" measure, however.

3.8 Disc Brake System

Standard aircraft disc type brakes assumed. The brake converts hydraulic pressure into braking torque on the wheel. The brake torque vs input hydraulic pressure characteristic curve was given in Chapter 2, Figure 6.

3.9 Wheel Speed Transducer and Torque Transducer

These sensors provide two of the signals necessary for the anti-skid system and slip controller to operate. Outputs of these sensors must be processed by A/D converters to allow interfacing with the computer. The A/D conversion interval is synchronized with the software routines and counter service sequence.

3.10 Mu-Slip Peak Detector and Maximum Slip Limiter.

Consider a family of characteristic mu-slip curves corresponding to various runway surface conditions, as shown in Figure 28.

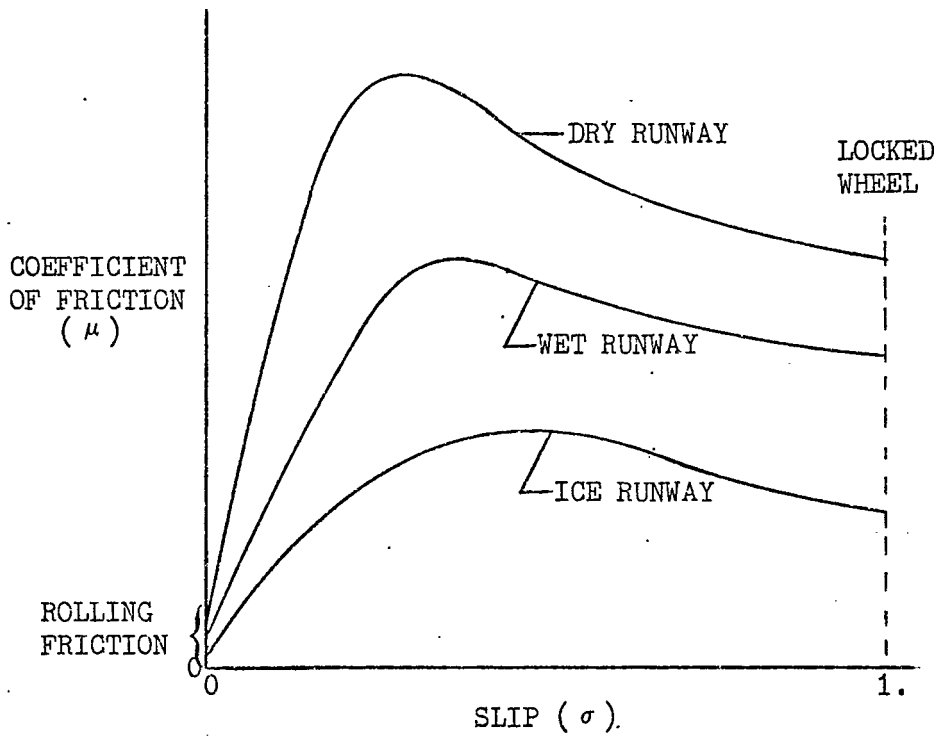


FIGURE 28. A FAMILY OF MU-SLIP CURVES.

These general observations can be made:

- The peak does not occur at a fixed slip value for all curves in the family.
- A σ of 1. corresponds to a locked wheel condition, and $\sigma = 0$ corresponds to a free rolling wheel.
- The region to the left of the peak can be considered as a non-skid region; to the right is a highly unstable skid region. This instability when operating to the right of the peak occurs due to the phenomena of decreasing friction with no increase in brake pressure. The mechanism of this instability is explained as follows. Assume for the moment that braking torque has exceeded the maximum ground force torque (T_{GF}), available at the peak of the mu-slip curve. Braking torque is a function of hydraulic brake pressure, which will now be held constant. And note that ground force torque is a function of the coefficient of friction. Now, as friction decreases (i.e. moving to the right of the peak), ground force torque decreases, which causes an increase in slip, thus further decreasing friction, and so the process repeats itself until ultimately the wheel locks up. Further, since this process is essentially a positive feedback system, it "diverges" rapidly. The time required to transverse the mu-slip curve from peak to wheel lockup (which can be less than 200 milliseconds) thus becomes one of the influencing factors in design

of a braking system.

Mu-Slip Peak Detector. The major problems encountered in sensing the peak of the mu-slip curve lies in the fact that mu cannot be measured directly. Slip can be reasonably approximated by Equation 3, which neglects flexure or stretching of the tire while undergoing braking.

The problem is reduced to finding a physical variable within the braking system which is either proportional to mu or a function of mu. Note that the product of mu and weight supported by a wheel determines the effective braking force for that wheel. Thus, if a means can be devised for measuring the braking force, then mu can be determined since weight on a given wheel is known (approximately). Two techniques for measuring ground force were investigated:

- (1) Measurement of reaction force seen by the landing gear strut, and
- (2) measurement of reaction torque seen by the brake mechanism.

The first method is most appropriate for vehicles having only one braked wheel per strut, whereas the second method is not influenced by the number of braked wheels per strut. In view of the fact that the Shuttle has two braked wheels per main gear strut, the reaction torque measurement technique is most applicable, and is developed as follows.

Consider first the mu-slip curve and its derivative ($d\mu / d\sigma$) as

shown in Figure 29.

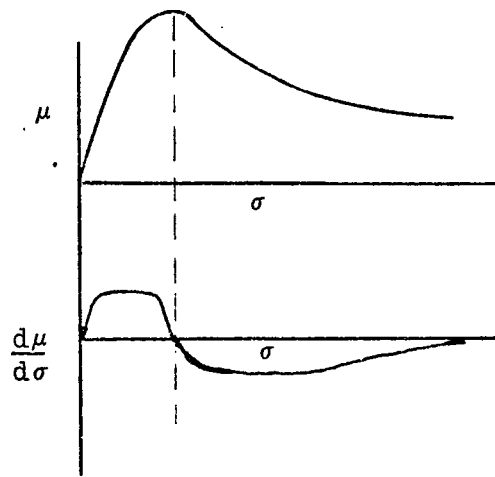


FIGURE 29. TYPICAL μ AND $d\mu/d\sigma$.

If some means of measuring slope ($d\mu/d\sigma$) of the curve can be devised, then obviously the point at which $d\mu/d\sigma$ passes through zero identifies the peak (excluding end points). The slope is related to measured torque as follows.

Consider the equation for slip,

$$\sigma = 1 - \omega / \omega_s \quad (38)$$

For small increments of time, the synchronous wheel speed can be assumed constant. Therefore, differentiating Equation 38 with respect to time yields:

$$\frac{d\sigma}{dt} = - \frac{1}{\omega_s} \cdot \frac{d\omega}{dt} \quad (39)$$

Next consider the torque which a transducer would read if it measured torque seen (reacted) by the brake mechanism:

$$\begin{aligned} T_M &= T_{GF} + J\dot{\omega} \\ &= \mu r W + J\dot{\omega} \end{aligned} \quad (40)$$

Where

T_M = measured reacted torque (ft-lb)

T_{GF} = ground force torque on the wheel, $\mu r W$ (ft-lb)

r = rolling radius of the wheel (1.5 ft)

W = weight on the wheel (lbs)

J = wheel moment of inertia (ft-lb-sec²)

ω = wheel speed (rad/sec)

Assume for the moment that the $J\dot{\omega}$ term can be neglected in Equation 40. Then, differentiating Equation 40 yields:

$$\frac{dT_M}{dt} = \frac{d(\mu r W)}{dt} \quad (41)$$

Now, for short increments of time, r and W can be assumed constant.

Therefore;

$$\frac{dT_M}{dt} = rW \frac{d\mu}{dt} \quad (42)$$

Dividing Equation 42 by Equation 39 gives the desired expression:

$$\frac{dT_M/dt}{d\sigma/dt} = \frac{rW(d\mu/dt)}{d\sigma/dt} \quad (43)$$

Simplifying:

$$\frac{d\mu}{d\sigma} = \frac{1}{rW} \cdot \frac{dT_M/dt}{d\sigma/dt} \quad (44)$$

Thus slope of the mu-slip curve is expressed in terms of variables which can be measured, namely reaction torque and wheel slip.

Next, consider the $J\dot{\omega}$ term (in Equation 40) which has been neglected thus far. Physically, this torque is inseparable from the ground force torque in terms of measurement, i.e. a torque transducer measures both T_{GF} and $J\dot{\omega}$ simultaneously and cannot distinguish between them. Therefore, in order to obtain an indication of true ground force torque, a value equal to $J\dot{\omega}$ must be subtracted from the measured torque. This can be done, since J of the wheel is a known quantity, and $\dot{\omega}$ can be determined from the wheel speed sensor.

$$\dot{\omega} = (\omega_t - \omega_{t-\Delta t})/\Delta t \quad (45)$$

This derivative will, of course, present the usual computed derivative "noise" problem.

Thus, ground force torque acting on the wheel is obtained by

subtracting a computer $J\dot{\omega}$ term from the measured brake reaction torque.

$$\begin{aligned} T_{GF}(\text{Computed}) &= T_M - J(\omega_t - \omega_{t-\Delta t})/\Delta t \\ &= T_{GF} + J\dot{\omega} - J(\omega_t - \omega_{t-\Delta t})/\Delta t \end{aligned} \quad (46)$$

Examination of Equation 44 indicates the logic to be used for peak detection:

$$\begin{aligned} \text{If } \left\{ \begin{array}{l} [\sigma(t) - \sigma(t - \Delta t)] > 0 \text{ and} \\ [T_{GF}(t) - T_{GF}(t - \Delta t)] > 0 \end{array} \right\} & : \text{ left of peak} \\ \\ \text{If } \left\{ \begin{array}{l} [\sigma(t) - \sigma(t - \Delta t)] > 0 \text{ and} \\ [T_{GF}(t) - T_{GF}(t - \Delta t)] < 0 \end{array} \right\} & : \text{ right of peak, and skid} \\ & \text{imminent.} \\ \\ \text{If } \left\{ \begin{array}{l} [\sigma(t) - \sigma(t - \Delta t)] > 0 \text{ and} \\ [T_{GF}(t) - T_{GF}(t - \Delta t)] = 0 \end{array} \right\} & : \text{ peak or "flat spot" in} \\ & \text{mu-slip curve.} \end{aligned}$$

The inability to distinguish between flat spots (or possible minor peaks) and the true peak of the mu slip curve will probably not present a practical problem. Wheel vibration, runway inconsistency and vehicle pitching/rolling motion should provide sufficient dither to keep the control system constantly active (searching for peak).

The mu-slip curve peak sensor is implemented as a software routine. Output of the routine is a count down discrete to the UP/DOWN Counter

whenever the peak is crossed in the direction of increasing wheel slip.

Maximum Slip Limiter. The purpose of this limiter is to insure that slip remain below some fixed limit under all circumstances. This limit would have to be determined from experimental data, and was arbitrarily set at .6 for testing in this thesis. The slip limiter is implemented via a software routine, and sends a count down discrete to the UP/DOWN Counter whenever the limit is exceeded. Note that, should the peak controller or slip command controller fail for any reason, the maximum slip limit controller automatically takes over the braking control function.

3.11 Steering Control Law

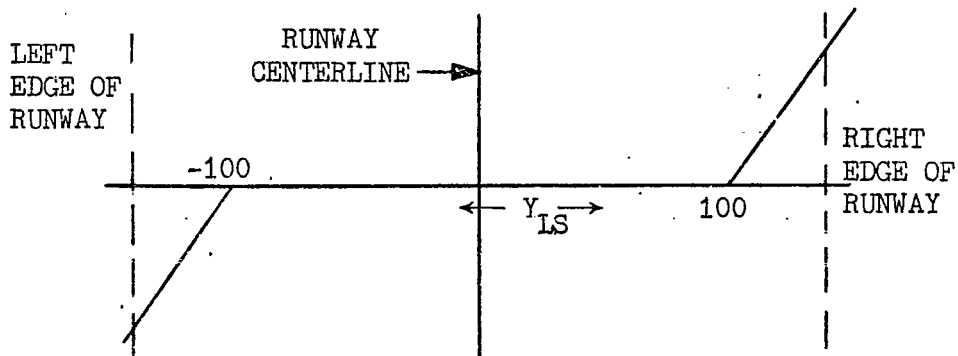
A steering control law is required to keep the vehicle on the runway during rollout. This control law must react rapidly to any angular deviation (yaw) away from a path parallel to the runway center line. Lateral translational deviations are not of such great concern, as long as the vehicle remains on the runway.

The steering law mechanized is:

$$\theta_{\text{steer cmd}} = - [\psi + (Y_{LS}/d_r) + \text{deadspace } f(Y_{LS})] \quad (47)$$

The term ψ causes a degree-for-degree effect, i.e. if the ψ body

rotation is one degree away from the runway center line, an opposite steering command of one degree is issued to the nosewheel and rudder. The Y_{LS}/d_r component causes steering to aim the vehicle towards a point which is on the runway center line at a distance equal to the stopping distance computed by the rollout estimator. Dead space $f(Y_{LS})$ is a term which acts only if the vehicle travels too far away from the runway center line and is in danger of running off the edge. The function is plotted below



Magnitude of the function is as follows

$$\begin{aligned}
 f(Y_{LS}) &= 0 \quad \text{for } -100' \leq Y_{LS} \leq 100' \\
 f(Y_{LS}) &= K(Y-100) \quad \text{for } Y_{LS} > 100' \\
 f(Y_{LS}) &= K(Y+100) \quad \text{for } Y_{LS} < -100'
 \end{aligned}
 \tag{48}$$

K can be adjusted to provide a desired steering command increment for each foot traveled beyond the ± 100 foot boundaries. For example, if

$K = 1$, then steering command is incremented .1 radian = 5.73 degrees for each foot of travel beyond the boundaries.

Steering is accomplished by means of the nosewheel and rudder. Braking of the main landing gear wheels could also be used for steering; however this method of directional control was not investigated.

The steering software routine is executed 20 times per second. Rudder and nosewheel steering actuators are not modeled; unity transfer functions are assumed for those devices.

3.12 Cockpit Controls and Displays

Pilot interface with the braking system is accomplished by the following items:

- Rudder/brake pedals, which directly command brake pressure in the MANUAL or the OVERRIDE mode of operation.
- AUTO/MANUAL mode select switch. This switch allows the pilot to choose whether the braking system will be completely automatic, or whether it will simply act as an antiskid protector for pilot (manual) braking. Cockpit indicator lights would show green if AUTO mode selected, or amber if MANUAL selected.
- OVERRIDE/NORMAL switch. This switch would only be placed in the OVERRIDE position in an emergency condition, i.e. if the primary braking control system should fail. There is no anti-skid protection in the OVERRIDE state and brake pedal commands are applied directly to the pressure control valve.

- ROLLOUT ESTIMATE DISPLAY. This digital display would show elapsed rollout distance, and the estimated rollout distance computed by the rollout estimator.
- WHEEL SLIP INDICATOR/SLIP COMMAND SELECTOR. The indicator portion would display wheel slip on a linear scale (0.0 to 1.0) for each braked wheel. The Slip Command Selector could be a thumbwheel switch, slide wire potentiometer, or rotary potentiometer, and would establish a slip value about which the automatic braking control system operates. Note that the pilot can control braking without using the brake pedals by adjusting the slip command setting, i.e. increasing slip command increases braking, and vice versa.
- SKID WARNING INDICATORS. A red light and buzzer should come on whenever the maximum slip sensor detects that maximum allowable slip is exceeded, or that μ -slip peak has been exceeded.

CHAPTER 4

TESTING, RESULTS AND CONCLUSIONS

4.1 System Testing

The automatic antiskid braking system design was tested to verify proper performance in all modes of operation. Performance factors of interest included:

- Achieve and hold a commanded (fixed) wheel slip value.
- Sense impending wheel skid and provide preventative action.
- Maintain braking control about the peak of the mu-slip curve when maximum braking is required.
- Sense runway surface condition and adapt to any changes (dry, wet, ice).
- Provide antiskid backup for pilot braking at all times.
- Provide completely automatic operation, i.e. estimate rollout distance and adjust braking such that vehicle stops within 6000 feet.
- Provide warning to pilot of impending wheel skid.

Tests were accomplished by changing modes of operation and runway conditions during run time. The simulation program has considerable flexibility "built in", allowing variation of the following parameters or conditions:

- Runway conditions (dry, wet, ice).
- Braking control system mode of operation (automatic or fixed slip command mode).

- Digital filters in or out, and variation of filter parameters.
- Counter service frequency, and magnitude of count increment/decrement of the UP/DOWN Counters.
- Frequency of mu-slip curve peak check.

Other parameters such as integration step size, initial positions and velocities, vehicle mass properties and dimensional data, and system constants are controlled via initial condition statements. The capability for varying parameters during run time greatly reduced computer usage, since repeated program compilation time was reduced.

A typical test sequence is shown in the following table:

<u>TIME OF SEGMENT (SEC)</u>	<u>RUNWAY CONDITION(S) (DRY, ICE, WET)</u>	<u>DIGITAL FILTER (IN OR OUT)</u>	<u>SLIP COMMAND MODE (AUTO OR FIXED)</u>
0-1	DRY	OUT	AUTO
1-2	ICE	OUT	AUTO
2-3	WET	OUT	AUTO
3-4.5	DRY	IN	AUTO
4.5-6	WET	IN	AUTO
6-7	DRY	IN	FIXED (.4)
7-8	DRY	IN	FIXED (.25)
8-9	DRY	OUT	FIXED (.25)

4.2 Results

Figure 30 shows several parameters of interest for the automatic mode of operation. Note that one second of real time data is shown; during this time the vehicle travels 288 feet down the runway, and velocity is reduced from 300 ft/sec to 293 ft/sec. This run started with essentially no braking applied, and steady state limit cycling braking operation is achieved within 0.5 seconds. Estimated rollout distance d_r varies about the desired 6000 foot value, and estimated time to stop is approximately 40 seconds. Commanded slip varies from .0504 to .1004. For this run, the maximum allowable slip command increment was 0.05; reducing this value will correspondingly reduce the limit cycle amplitudes of all variables. Ideal measurement of ground force is assumed for this run.

Figure 31 indicates the ability of the peak riding controller to sense and track the peak of the μ -slip curve. This performance is typical for dry, wet, or ice pavement. Note that wheel slip peak-to-peak excursions are only 3.5 percent of full range. The plot for coefficient of friction shows little activity because the μ -slip curve being used is fairly flat near the peak.

Figure 32 shows system response to a fixed slip command of 0.25 both with and without digital filters on the outputs of the UP/DOWN Counters. Note that data is shown for two different low pass filters; one with a break frequency at 5 Hz, and the other at 100 Hz. Response with the 5 Hz filter is considered unacceptable due to the large excursions of wheel slip. Response with the 100 Hz filter shows

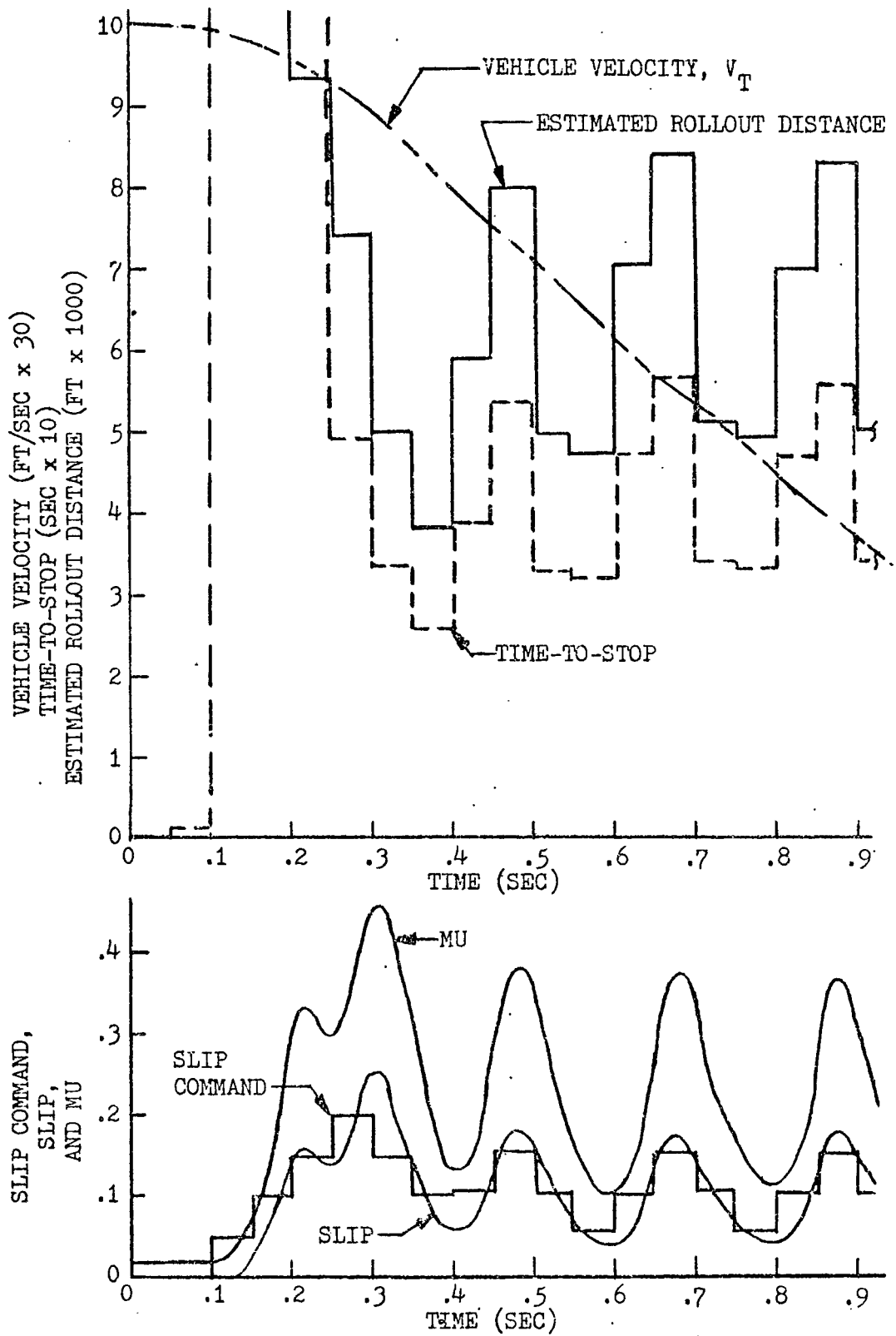


FIGURE 30. SYSTEM PERFORMANCE IN AUTOMATIC MODE.

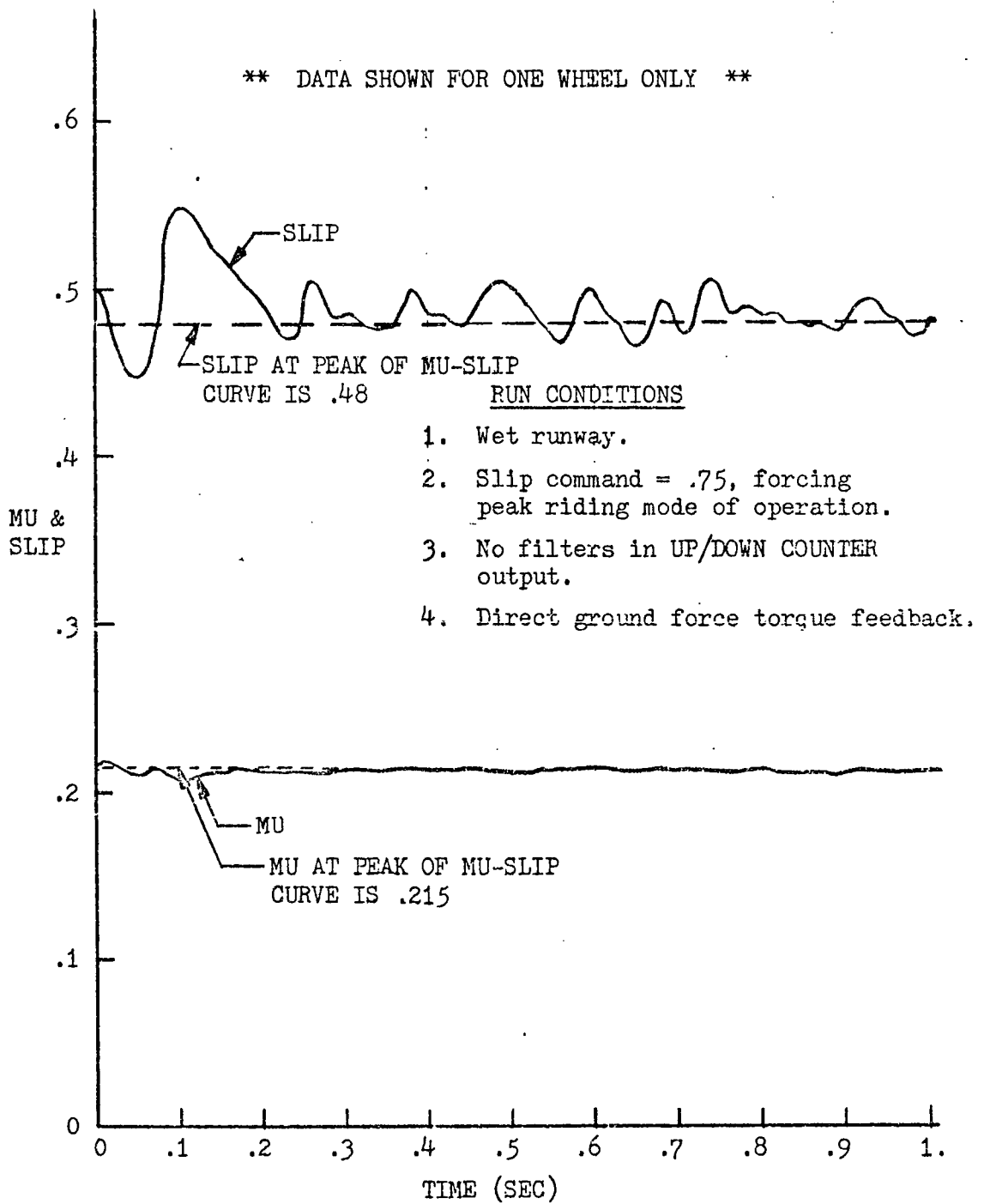
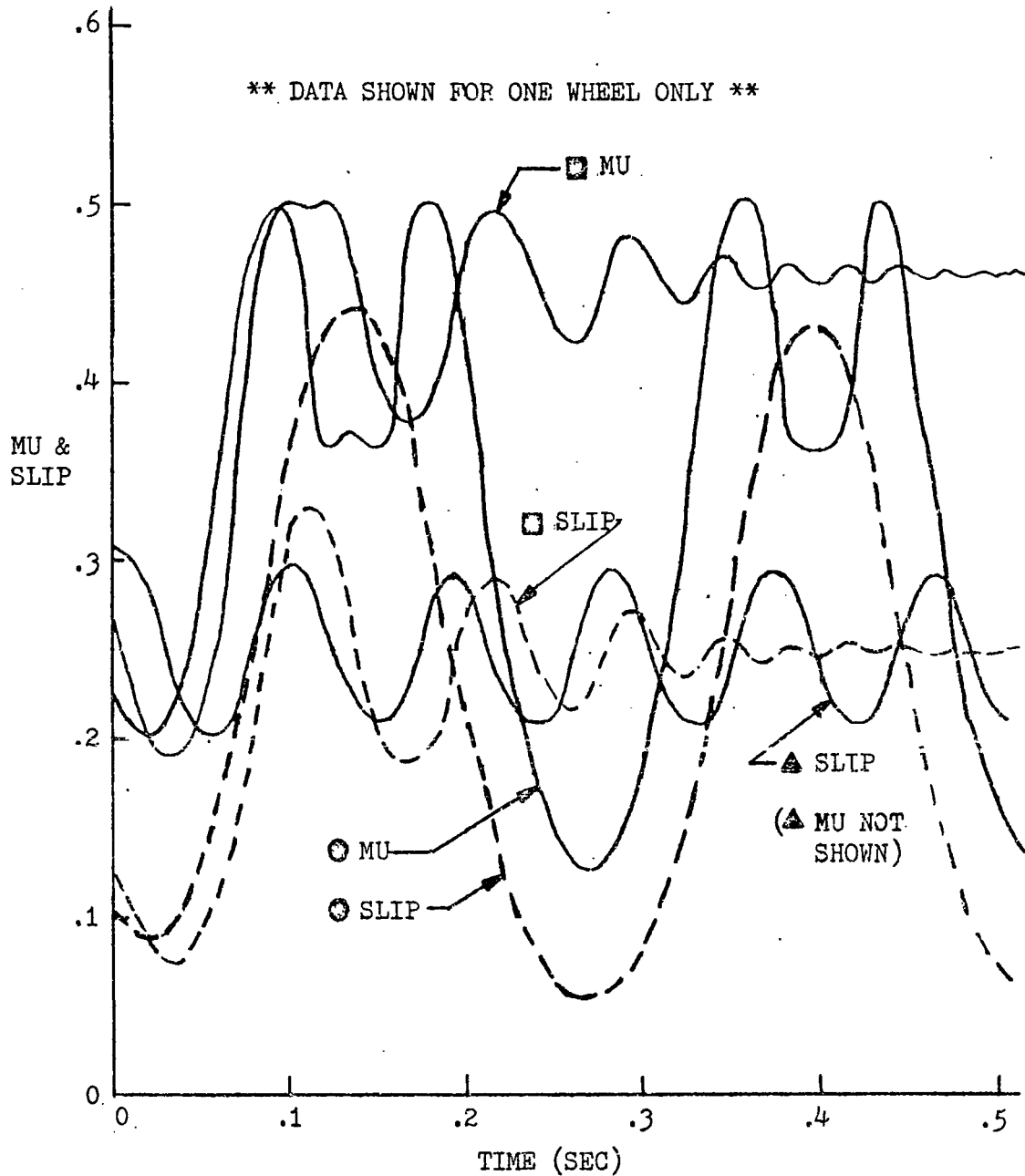


FIGURE 31. MU AND SLIP DATA FOR PEAK RIDING PERFORMANCE ON WET RUNWAY.



LEGEND:

- Dry runway; No filter in counter output.
- Dry runway; 5 Hz filter in counter output.
- ▲ Dry runway; 100 Hz filter in counter output;
(Only slip is plotted for this case.)

FIGURE 32. MU AND SLIP RESPONSE DATA FOR FIXED SLIP COMMAND OPERATION (SLIP COMMAND = .25).

considerable improvement in terms of wheel slip variation. However, the near perfect sinusoidal limit cycle oscillation at approximately 11 Hz would probably excite landing gear mechanical oscillations. Thus it must be concluded that operation without any filtering of UP/DOWN Counter outputs is preferable. Note that, without filtering, the actual wheel slip is well within $\pm 1\%$ of commanded value.

Results of a test involving computed ground force torque is shown in Figure 33. Computed torque requires derivation of wheel acceleration based upon differentiation of measured wheel speed data. This computed derivative proved to be quite noisy, as is the usual case for derivative type signals. For this particular test the slip command was set at a high value to insure that the system would automatically assume the peak riding mode of operation. Note that the peak check test was made every .0001 second for this particular run; peak checking at .01 second intervals produced erratic performance due to the noisy $J\dot{\omega}$ data. The system stabilized at a slip value approximately 5 percent above the value for the peak of the mu-slip curve.

Data in Figure 34 shows results of an attempt to smooth the computed ground force feedback term with a 50 Hz filter. The system achieved a limit cycle operation mode about a slip of approximately .53, which is 20 percent above the peak slip value. This would, of course, be an unacceptable operating region. Data of Figures 33 and 34 are shown simply to highlight the problem of measuring a true ground force signal.

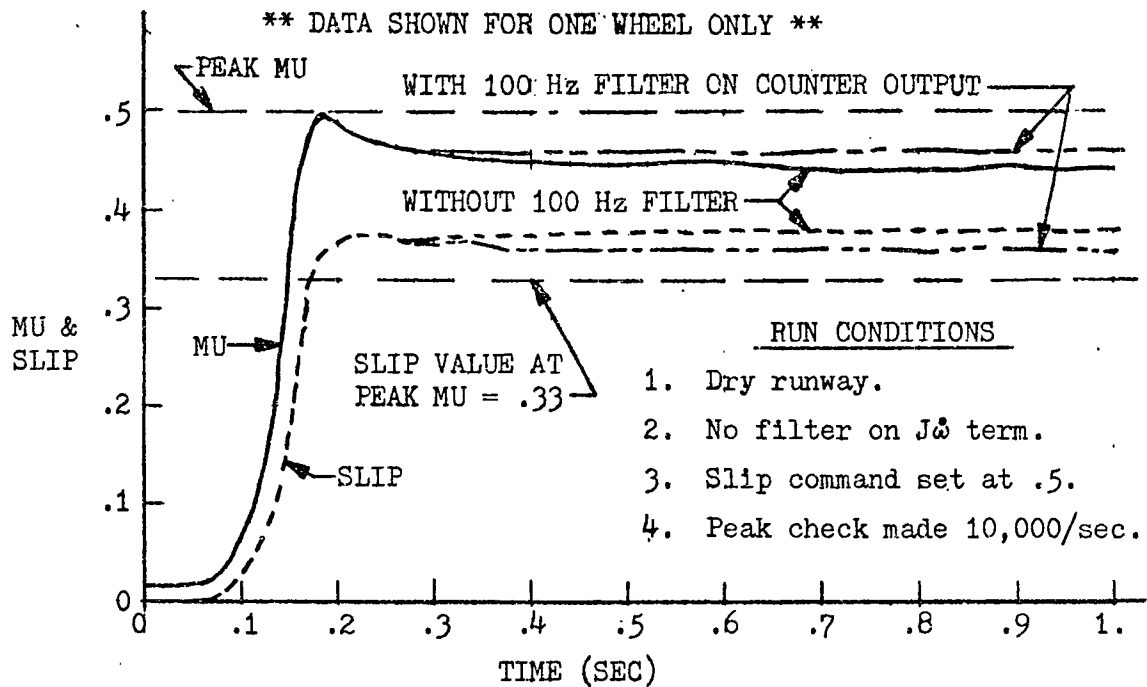


FIGURE 33. MU AND SLIP RESPONSE FOR SYSTEM OPERATION WITH COMPUTED CANCELLATION OF $J\dot{\omega}$ TERM.

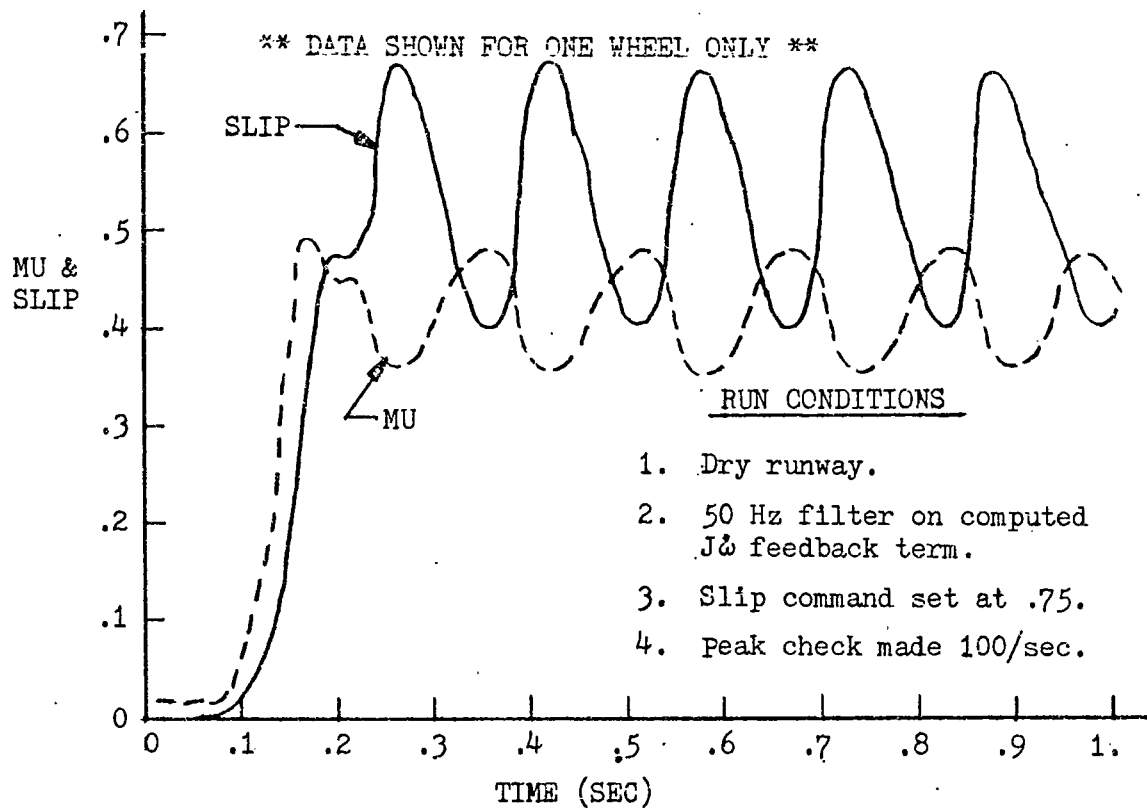


FIGURE 34. MU AND SLIP RESPONSE FOR SYSTEM OPERATION WITH COMPUTED CANCELLATION OF $J\dot{\omega}$ TERM .

Time required to lock a wheel ($\omega=0$) once the peak of the mu-slip curve has been exceeded is indicated by the data in Figure 35. This test was conducted by allowing the brake pressure to build up to a value which caused the peak to be exceeded. As soon as the peak detector sensed that the peak had been exceeded the counter output was frozen at its last value. Thus braking pressure was only a few percent above that required to exceed the peak of the mu-slip curve. This data represents dry runway response.

Figure 36 shows typical steering control law performance over a distance of approximately 1100 feet. The disturbance torque causing lateral travel is uneven braking (one wheel supported 5000 pounds more than the other). For this particular run the steering control law deadspace limit was set at ± 4 feet to demonstrate control ability. In a practical situation this limit would probably be set at approximately 100 feet.

4.3 Conclusions

The fundamental conclusion of this thesis is that the automatic antiskid braking control system concept as presented is a feasible system. Peak detection of the mu-slip curve using measured wheel slip and braking reaction torque provided good results; the most difficult problem to overcome in implementing this scheme would be measurement of wheel acceleration which is used to compute a value of effective ground force torque. Probably the most practical solution

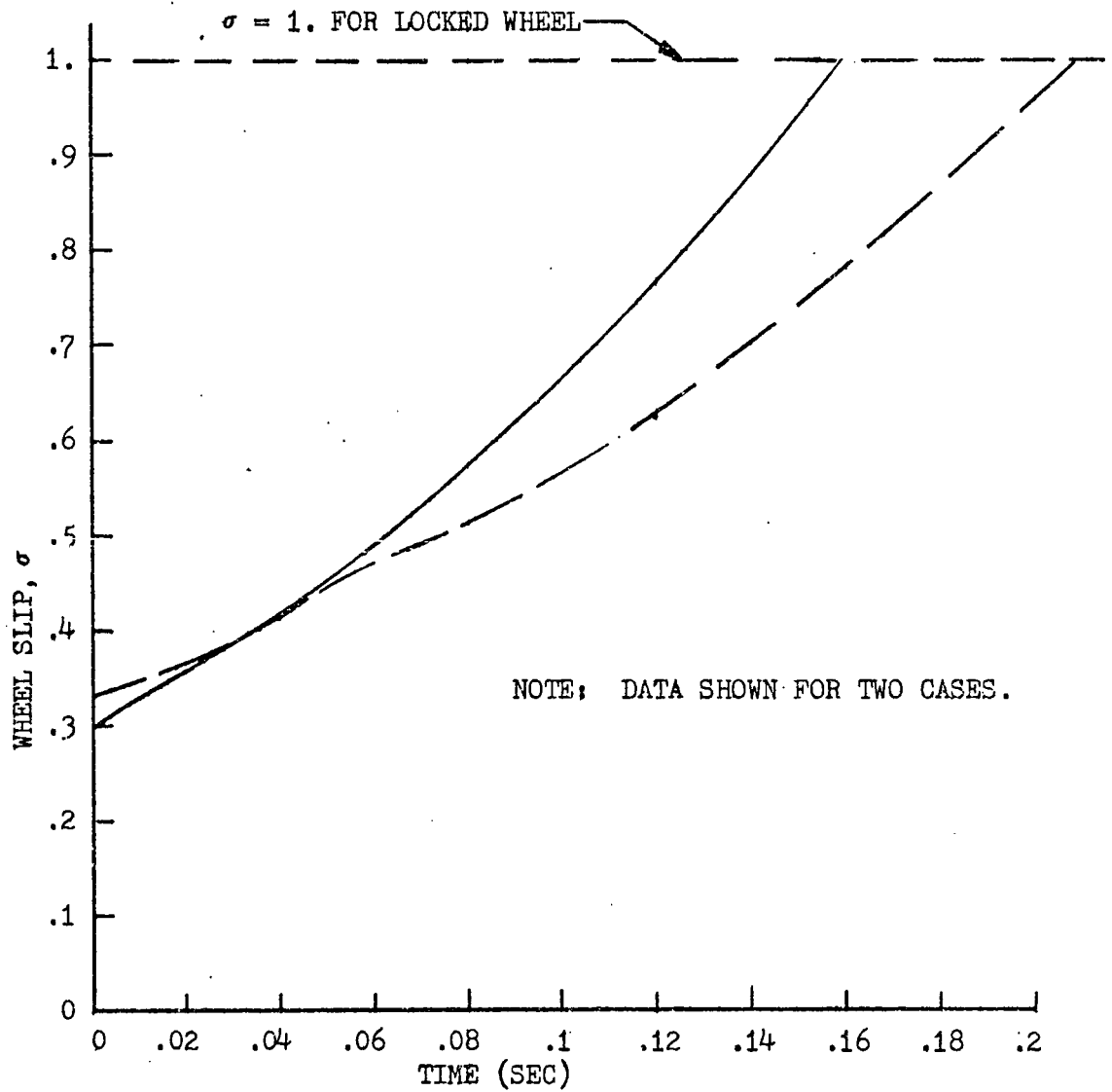


FIGURE 35. TYPICAL WHEEL LOCKUP CHARACTERISTICS WITH EXCESSIVE BRAKING PRESSURE APPLIED.

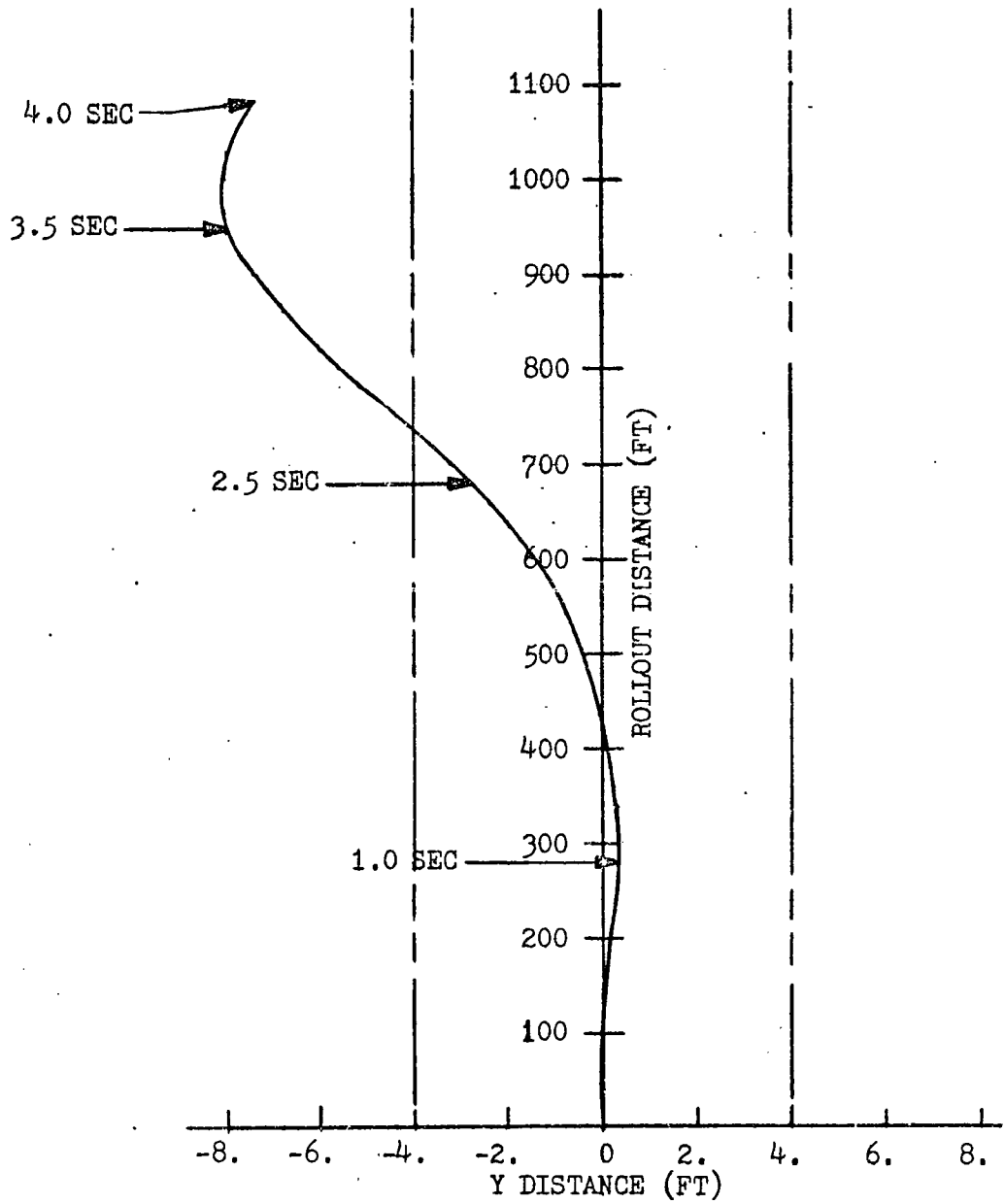


FIGURE 36. STEERING CONTROL EFFECTIVENESS DATA.

to this problem would be passive filtering (R, L, C components) of the wheel speed signal combined with a digital filter in the software routine which computes wheel speed acceleration.

The combination rollout estimator/slip command controller concept provides very good braking control, with the system tracking commanded slip to within $\pm 1\%$. This scheme also allows straightforward pilot interface via a slip command control device such as a potentiometer or thumbwheel selector switch. Steering via braking could also be readily mechanized via slip command as shown in Figure 37.

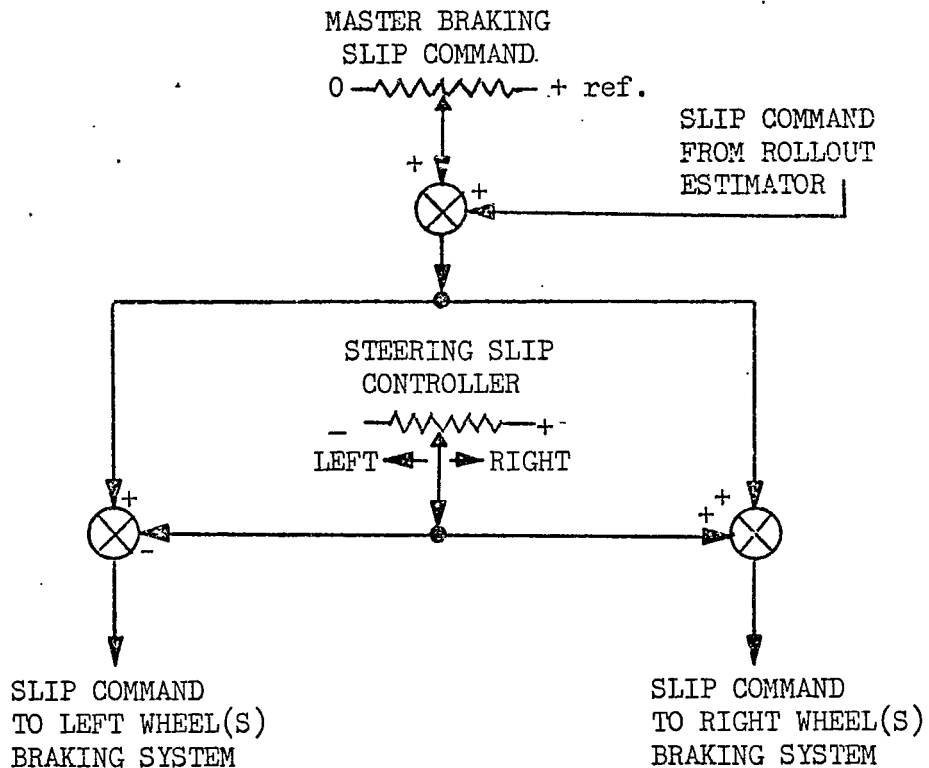


FIGURE 37. STEERING VIA MAIN GEAR BRAKING.

Steering would be accomplished by adding a slip command bias to the braking controllers for one set of wheels, (right or left), and subtracting a similar bias term from the opposite side. These bias terms would add to and subtract from the master braking slip command.

Smoothness of braking while operating in the automatic braking control mode is influenced by several factors, including:

- Shape of the mu-slip curve.
- Quantization (resolution) of command variables.
- Iteration rates of various software routines in the control system.

True shape of the mu-slip curve at any given time is a virtual unknown, i.e. uncontrollable. The latter two items are controllable and can be adjusted to achieve a desired level of smoothness and response time. "Smoothness" refers to the magnitude of change in braking forces due to variations in slip (and hence mu). If the slip command signal is only allowed to change in small increments (say less than .05, then braking will be relatively smooth on a constant runway. Indeed, if the runway is truly constant, the commanded slip will tend to a fixed value, providing constant braking. Restricting the maximum value by which the slip command can be incremented results in increased response time. Thus the time to establish a command value following touchdown (conceivably several seconds) and to adjust to changing runway conditions may be unacceptable. This response time can be speeded up by increasing rollout estimator iteration rate. However,

since the system typically requires approximately .5 seconds to stabilize to a new commanded slip value, the iteration rate should not exceed (be faster than) two per second.

Digital filtering (5 Hz low pass roll-off) of the UP/DOWN Counter outputs proved effective in reducing high frequency oscillations of the braking control loop. However, the price paid in response time is too great in terms of wheel slip variations. Frequency response of the filter had to be increased to more than 100 Hz to achieve acceptably small slip variation during limit cycle operation. Best response was achieved with the filter out of the loop. It is therefore concluded that limit cycle frequency and/or amplitude of the braking control loop can best be controlled by UP/DOWN Counter control logic. For example, forcing the counter to count down for .050 seconds (50 iterations at a 1 KHZ service rate) any time the mu-slip sensor detects a peak would insure a 10 Hz or less frequency of oscillation about the peak. Similar logic could be implemented when operating about a fixed slip command.

A final conclusion is that the various models developed for this thesis should be quite useful for investigating the many questions still to be answered regarding automatic antiskid braking control systems.

BIBLIOGRAPHY

1. "Preliminary Investigations on an Automatic Braking Control System for the Space Shuttle", NASA Internal Note MSC-EG-71-34, by Dr. Eugene D. Denman, University of Houston, November 3, 1971.
2. Communications with Mr. Orland D. Branson, Senior Staff Engineer, Bendix Company, Electrodynamics Division, Sylman, California.
3. "Optimal Braking Studies", John S. Pazdera, University of Missouri at Rolla, August, 1972.
4. "Research Study on Antiskid Braking Systems for the Space Shuttle", by J.A. Auselmi, L. W. Weinberg, R. F. Yurczyk, and W. G. Nelson, The Boeing Company Document No. D6-41115, 1973.
5. "Requirements Definition Document", No. SD-72-SH-0102, by Rockwell International Corporation, June, 1973.
6. "System/360 Continuous System Modeling Program Users Manual", Program No. 360A-CX-16X, Document No. GH-20-0367-4, by the IEM Corporation.
7. "Theory of Sampled Data Control Systems", by David P. Lindorff, 1965.